(U-Th)/He, U/Pb, and Radiation Damage Dating of the Rochechouart-Chassenon Impact Structure, France

by

Audrey Horne

A Thesis Presented in Partial Fulfillment
of the Requirements for the Degree
Master of Science

Approved July 2016 by the
Graduate Supervisory Committee:

Kip Hodges, Chair
Matthijs van Soest
Axel Wittmann

ARIZONA STATE UNIVERSITY

August 2016

ABSTRACT

It has been hypothesized that the ~25 km Rochechouart-Chassenon impact structure (RCIS) in the NW Massif Central, France, was formed during a Late Triassic (ca. 214 Ma) terrestrial impact event that produced a catena of several large craters. Testing this hypothesis, and assessing its possible impacts on biological evolution, requires both accurate and precise dating of candidate impact structures. Like many of these structures, the age of the RCIS is controversial because geochronological datasets yield contradictory results, even when a single isotopic system is used; for example, the two most recent $^{40}Ar/^{39}Ar$ studies of RCIS yielded statistically inconsistent dates of 201 ± 2 Ma (2σ) and 214 ± 8 Ma (2σ). While the precision offered by various geochronometers used to date impact structures varies significantly, a fair way to assess the confidence scientists might have in the accuracy of an impact age is to establish whether or not multiple chronometers yield statistically indistinguishable ages when applied to that structure. With that in mind, I have applied the (U-Th)/He, U/Pb, and radiation damage chronometers to zircons separated from two different RCIS impactites. My best estimate of the zircon (U-Th)/He age of the impact event is 191.6 ± 9.1 Ma at the 95% confidence level. U/Pb zircon dates suggest that most zircons in the RCIS target rocks were not completely reset during impact, but a subset (n = 8) of zircons appear to have crystallized from the impact melt or to have been completely reset; these zircons indicate a U/Pb impact age of 202.6 ± 5.8 Ma (95% confidence level). Zircon radiation damage dates are highly variable, indicating that the RCIS event resulted only in partial annealing of pre-impact zircon in the country rock, but a small sub-population of zircons yielded a mean date of 211 ± 13 Ma (95% confidence level). These results – all statistically indistinguishable from the previously published $^{40}Ar/^{39}Ar$ date of 201 ± 2 Ma – collectively argue that the impact age was near the presently agreed upon Triassic-

Jurassic boundary. This age raises the possibility that seismite and tsunamite deposits found in the present-day British Isles may be related to the RCIS.

ACKNOWLEDGMENTS

I would like to thank my committee members for all of their advice and support through this project, especially my advisor Dr. Kip Hodges, who was very helpful and understanding throughout this process. Their knowledge was invaluable to my success. I also would like to thank Dr. Philippe Lambert for guiding me through fieldwork and providing a wealth of information on the impact crater. I would like to thank Michelle Aigner for consistently being available to aid me with lab work. Finally, I would like to thank the Barringer Family Fund for Meteorite Impact Research, and especially Dr. David Kring, for providing the travel funds for my project, which allowed me to collect my own samples for analysis.

TABLE OF CONTENTS

LIST OF TABLES

LIST OF FIGURES

INTRODUCTION

Spray et al. (1998) proposed that the Rochechouart-Chassenon impact structure (RCIS) in France was part of a terrestrial crater chain – or *catena* – similar to the one produced on Jupiter during the 1994 impact of comet Shoemaker-Levy 9 (Weaver et al. 1995; Orton et al. 1995). Based on geochronological evidence available at the time, they proposed that five known terrestrial craters – Manicouagan and Lake St. Martin in Canada, Obolon' in Ukraine, Red Wing in U.S.A., and RCIS – were coeval at ca. 214 Ma and serve witness to the event. However, new $^{40}Ar/^{39}Ar$ data for RCIS impact-metamorphosed target rock published by Schmieder et al. (2010) indicated a 201 ± 2 Ma age, and the authors used this finding to argue against the catena model. Given that this interpretation is based solely on Ar systematics and that previous estimates based on other chronometers (as well as other $^{40}Ar/^{39}Ar$ data) and paleomagnetics remain consistent with the catena interpretation, we were motivated to apply the (U-Th)/He and U/Pb methods to zircons from representative RCIS impactite samples in order to test the competing hypotheses.

The zircon (U-Th)/He thermochronometer (ZrnHe) is potentially valuable for such a study because the He diffusion kinetics of zircon predict that a high percentage of the pre-impact zircon crystals in impact target rock might yield (U-Th)/He dates concordant with the age of the impact given the size of the RCIS (Young et al. 2013). Although the (U-Th)/He systematics of zircon are also susceptible to partial or complete resetting during post-impact metamorphism or hydrothermal activity, there is no known post-impact thermal overprint in the RCIS region (Schmieder et al. 2010). The U/Pb zircon (ZrnPb) geochronometer may also be applied to impactite zircons, but has been only occasionally successful for impact event dating due to the very sluggish diffusion of

Pb in zircon (Young et al. 2013). However, there are some examples of successfully dated impact events using this system, both on Earth and on the Moon (e.g. Krogh et al. 1984; Hodych and Dunning 1992; Kamo et al. 1996; Hart et al. 1997; Davis 2008; Zhang et al. 2011; Norman and Nemchin 2014).

An important potential outcome of this study, and for any chronological study of a major impact structure, is the generation of information that would support correlation of an impact event with a global or regional biological extinction—like the significant discovery that the Chicxulub impact might have caused one of the most devastating biological extinctions in Earth's history at the Cretaceous-Tertiary boundary (Alvarez et al. 1980; Hildebrand et al. 1991; Schulte et al. 2010). However, precise dating of both events is necessary for correlation. Many impact craters are roughly dated via stratigraphy and, even if their permissible dates overlap with an extinction event, the ages may be too imprecise to confidently establish a link between the events. Schmieder et al. (2010) also proposed a correlation between RCIS and tsunami deposits found in the British Isles due to their updated Rhaetian age (Simms 2003, 2007); this study's dataset will also serve to address the consistency of this postulated connection.

GEOLOGIC BACKGROUND

The RCIS is located 40 km west of Limoges in the Limousin region of central France. The original crater is estimated to have had a diameter of ~25 km, but it currently has no topographic expression due (especially) to significant Quaternary glacial erosion (Kraut and French 1971; Lambert 1977). The degree of erosion is such that it is now possible to observe the crater floor. Although its size implies that RCIS was a complex crater (in the terminology of Dence 1964), there is no surviving evidence of the

central peak that is characteristic of such structures (Lambert 1974a, 1982; Melosh 1989). Like most rocks found associated with impact craters, the Rochechouart impactites were originally interpreted as volcanic deposits (Manes 1833, as referenced in Kelley and Spray 1997), but Kraut and co-workers correctly interpreted Rochechouart as a terrestrial impact crater in the 1960s based on impact shock features (Kraut 1967, 1969; Kraut and French 1971). At the time of impact, the target rocks for the RCIS were located in a shallow-water part of the Tethys Sea, as evidenced by paleogeographic reconstructions and the observation that Triassic and Lower Jurassic marine sedimentary rocks of the Aquitaine Basin are found only 20-25 km WSW of its present coordinates (Lambert 1977, 2010; Ziegler 1988).

The Rochechouart-Chassenon impact occurred in crystalline rocks of the northwestern Massif Central sector of the Variscan orogenic system (Figure 1). While predominant lithologic units in the impact region have been mapped as granite and gneiss, a variety of other rock types also occur, including subordinate diorite, gabbro, amphibolite, and serpentinite (Lambert 1977, 2010; Reimold et al. 1983). Massif Central was situated at the northern Gondwana margin and, prior to the Variscan orogeny, this region endured the opening and closing of various oceanic domains, which resulted in diachronous magmatic events during the Cambrian and Early Ordovician (Alexandre 2007; Melleton et al. 2010 and references therein). The resulting intrusions are thought to be the protoliths for orthogneiss in the Lower and Upper Gneiss Units (LGU and UGU, Figure 1) in the northwest Massif Central (Alexandre 2007; Melleton et al. 2010). The LGU and UGU are the middle stratigraphic units in a series of four stacked nappes (Faure et al. 2005; Melleton et al. 2010). The metamorphism associated with the nappe stacking event occurred during the Middle Devonian (Ledru et al. 1989 as referenced in

Melleton et al. 2010; Faure et al. 2005); however, the metamorphic event (or events) are not substantially reflected in U/Pb geochronometry for the LGU and UGU (Alexandre 2007; Melleton et al. 2010). Instead, the majority of orthogneiss $^{206}Pb/^{238}U$ dates are interpreted as protolith ages: LGU orthogneiss ~70 km southeast of the crater yielded a date of 451 ± 5 Ma (Melleton et al. 2010), which is supported by another LGU orthogneiss ~40 km west of the crater that yielded three major zircon populations at 457 ± 23 Ma, 526 ± 14 Ma, and 617 ± 17 Ma (Alexandre 2007). Melleton et al. (2010) also analyzed an UGU orthogneiss ~100 km northeast of the crater that yielded a U/Pb zircon date of 574 ± 14 Ma. Alexandre (2007) interprets the Neoproterozoic population as relating to Cadomian orogenic magmatism, the Cambrian population as magmatism during the recycling and reworking of Gondwana-derived basement blocks, and the Ordovician population as magmatism during oceanic subduction. The six youngest detrital zircon grains from a sample of UGU paragneiss collected ~120 km northeast of the crater indicated a maximum depositional date of 558 ± 9 Ma for its sedimentary protolith (Melleton et al. 2010). However, the sample also contains older inherited grains that range from 713 to 3,100 Ma, which are thought to reflect a West African cratonic source (Melleton et al. 2010). LGU paragneiss ~100 km southeast of the crater contained zircons with U/Pb dates as young as 573 ± 12 Ma, with a significant proportion of inherited grains having dates of 670 to 2,800 Ma (Melleton et al. 2010). Collectively, the datasets from Melleton et al. (2010) and Alexandre (2007) demonstrate that LGU and UGU zircon U/Pb dates typically range between the Ordovician and Archean. The only existing date for a target rock granite within the RCIS is 265 ± 12 Ma (2σ, Rb/Sr, Reimold et al. 1987). This is technically post-Variscan magmatism and there are no other reports of plutonic rocks in the northwestern Massif Central that are quite this young

(Lambert 2010). The closest dated extra-crater granitoid is 315 ± 17 Ma (Rb/Sr) on the St. Mathieu granite (Duthou 1977 as referenced in Duthou et al. 1984), but Alexandrov et al. (2000) demonstrated that many intrusions in the northwestern Massif Central were emplaced between 325 and 300 Ma, presumably during late-orogenic extension.

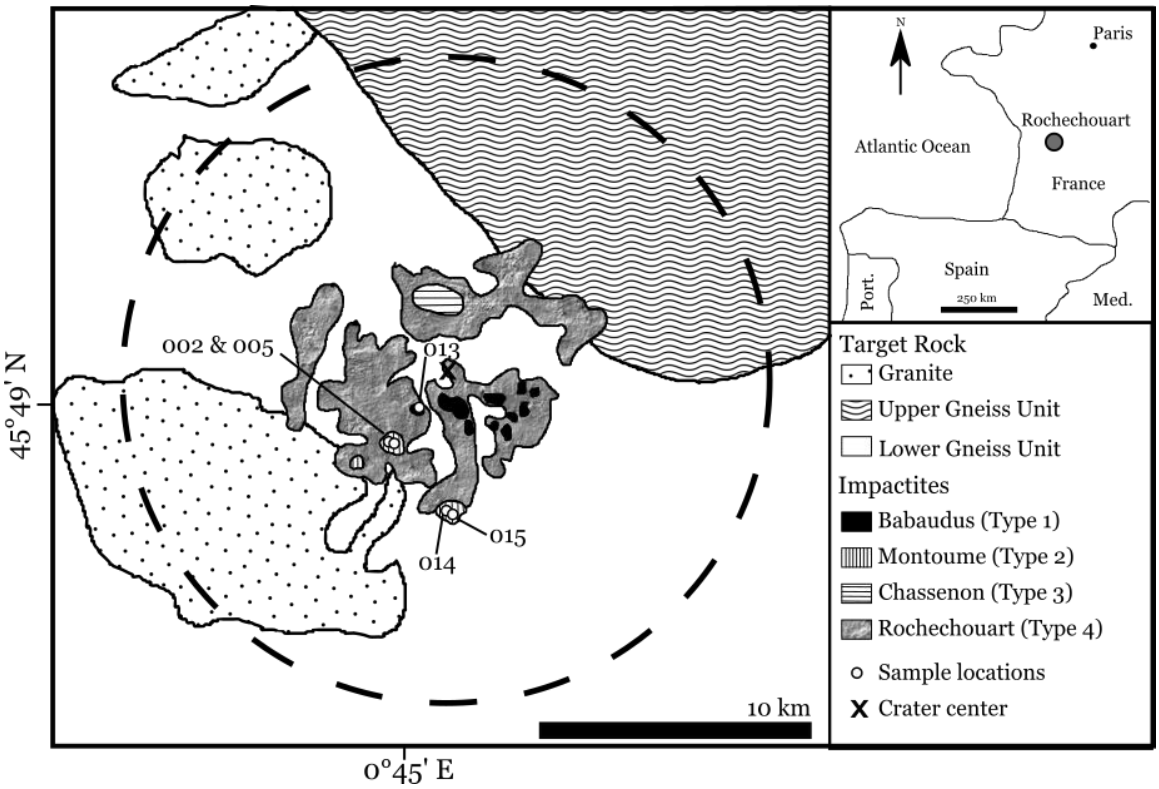

Figure 1: Simplified geologic map of the RCIS. Impactite locales are modified after Kelley and Spray (1997); target rock locales are modified after Lambert (2010), Locations for samples collected in this study are indicated on the map. For impactite descriptions, see Table 1. Dashed line indicates the ~25 km crater diameter.

The character of the RCIS impactor is still debated. Noting siderophile enrichment in some of the impactites, Janssens et al. (1977) proposed that it was a IIA iron meteorite. Additional geochemical data subsequently led others to instead suggest that the projectile was chondritic (Horn and El Goresy 1980; Koeberl et al. 2007). Tagle et al. (2009) again inferred that the impactor was an iron meteorite based on platinum

group elemental abundances and siderophilic ratios of the impactites. However, many still accept the chondritic impactor interpretation (Lambert 2010).

The impactites found at RCIS are more heterogeneous than those found at larger craters like Manicouagan, where the melt sheet is continuous (Palme et al. 1978; Horn and El Goresy 1981; Lambert 2010). They are notoriously difficult to classify, as they are often dissimilar to impactites from other structures that were used to build the canonical impactite nomenclature (Sapers et al. 2014 and references therein). Four main types of lithologies have been identified within the mantling deposits of the shocked and fractured autochthonous basement rock at RCIS: 1) glassy, buff-colored impact melt with shocked and altered clasts; 2) polymict breccia with a vibrantly red, devitrified glassy matrix and shocked clasts; 3) polymict breccia with a glassy green matrix and shocked clasts; and 4) glass-free monomict breccia with shocked clasts (Table 1, French and Kraut 1971; Lambert 1977). Locally, these impactites have been given the names Babaudus, Montoume, Chassenon, and Rochechouart, respectively. Alternative descriptions of these units, suggested by Sapers et al. (2014), are also included in Table 1. The Chassenon breccia is likened to the high-temperature suevite deposit found at Ries crater, while the Rochechouart breccia is likened to the low-temperature Ries suevite (French and Kraut 1971; Horn and El Goresy 1980, 1981). All RCIS impact rocks are enriched in potassium relative to the target rock (on average, 5-7 wt% more K_2O), an observation which has been interpreted in terms of impact-induced K-metasomatism during widespread post-impact hydrothermal activity (Lambert 1977, 2010; Reimold et al. 1984, Schmieder et al. 2010).

PREVIOUS ESTIMATES FOR THE AGE OF THE IMPACT EVENT

K/Ar

Fundamental geologic relationships in the area constrain the RCIS to be post-Variscan. The first direct dates for the RCIS impactites were reported by French and Kraut (1971). They interpreted unpublished K/Ar dates of 154 ± 8 and 173 ± 8 Ma (2σ) for the Babaudus impact melt rock – "personal communication" from J.B. Hartung – as constraining the minimum age of the impact. These results were broadly reproduced independently by Lambert (1974b): 165 ± 10 Ma (2σ, n=2). All of these dates were published before the 1976 IUGS Subcommision on Geochronology (Steiger and Jäger 1977) subsequently recommended new values for ^{40}K decay constants and K isotopic abundances that are in common use today. The Babaudus K/Ar results from both publications are shown in Table 2, recalculated using the Steiger and Jäger (1977) values.

Rb/Sr

Reimold and Oskierski (1987) introduced a new age of 185.5 ± 8.4 Ma (2σ, $(^{87}Sr/^{86}Sr)_{initial}$=0.7116 ± 0.0009) for Rochechouart based on application of the Rb/Sr chronometer to a sample of the Babaudus impact melt rock. They analyzed a combination of whole rock, acid-leached fluid, pyroxene concentrate (pyroxene + mesostasis), and feldspar (sanidine); however, the isochron date is solely represented by seven analyses that are a combination of the residues and fluids from a single whole rock sample that endured three acid-leaching steps. Although samples were leached, they reported that the isochron regression was a mixing line between impact melt and alteration products.

Reimold et al. (1987) dated a pseudotachylite vein from the Champagnac quarry

Table 1: Impactites of the RCIS.

Type	Known as	French and Kraut (1971)	Sapers et al. (2014)
1	Babaudus (B)	Crystalline melt rock with scattered shocked and altered clasts	Clast-poor impact melt with a crystalline matrix
2	Montoume (M)	Red-welded breccia with shocked clasts in dense welded and recrystallized glassy matrix	Clast-rich particulate impact melt rock with a crystalline matrix
3	Chassenon (C)	Glass-bearing breccia with shocked and altered lithic clasts	Melt-bearing impact breccia with a clastic groundmass and melt/glass-bearing inclusions
4	Rochechouart (R)	Lithic breccia with shocked clasts, sans glass	Lithic impact breccia

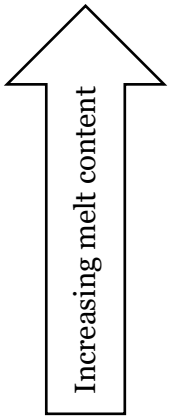

that yielded an isochron date of 217 ± 16 Ma (2σ, n=7) and initial $^{87}Sr/^{86}Sr$ ratio of 0.716 ± 0.004. This is distinguishable from the more-precise Reimold and Oskierski (1987) Babaudus age. Reimold and co-workers interpreted this date as a geologically insignificant "chance" array, and concluded that it was not representative of a mixing line between target rock and alteration products. They preferred the younger, more-precise Rb/Sr date from Reimold and Oskierski (1987) as indicative of the impact age.

Fission Track

Wagner and Storzer (1975) analyzed both glasses and apatites from the Chassenon impactite using the fission-track method. The glasses were separated from the matrix, while the apatites were separated from ~2 cm crystalline inclusions. Their initial findings were 69 ± 2 Ma and 168 ± 7 Ma for the glasses and apatites, respectively. However, they indicated that these dates were minima due to partial track fading during a subsequent thermal event. Employing calibration curves, they adjusted their fission-track dates to 206 ± 39 Ma for the glasses and 198 ± 25 Ma for the apatites (2σ).

$^{40}Ar/^{39}Ar$

The two most recently published ages for RCIS impactites were obtained using the $^{40}Ar/^{39}Ar$ method by Kelley and Spray (1997) and Schmieder et al. (2010). Kelley and Spray presented infrared (Nd-YAG) laser spot-fusion data for a ~1.5 cm-wide pseudotachylite vein from the Champagnac quarry in the northeast of the structure. Twenty-three matrix analyses range from 231 Ma to 1,686 Ma. They interpreted a 214 ± 8 Ma date from an isochron with eight 'central zone' matrix analyses as the impact age; this zone was relatively clast-poor compared to the outer edges of the vein. The isochron mean squared weighted deviation (MSWD; Wendt and Karl 1991) is 1.5, which is within the acceptable error for a population of eight analyses.

Schmieder et al. (2010) dated K-feldspar from an impact-metamorphosed gneiss basement rock using conventional step-heating methods. They analyzed primary, recrystallized K-feldspar of spherulitic texture and secondary, idiomorphic adularia that grew in cavities of the gneiss. The primary feldspar yielded an 8-step isochron date of 201.1 ± 1.8 Ma (2σ, ~80% ^{39}Ar), with an acceptable MSWD of 0.79, while the secondary feldspar yielded a slightly younger, but statistically indistinguishable 10-step isochron date of 200.1 ± 3.8 Ma (2σ, ~85% ^{39}Ar), with an acceptable MSWD of 0.51. The isochrons indicated ^{40}Ar/^{36}Ar ratios of 298 ± 10 and 300 ± 36 for the primary and secondary feldspars, respectively. The overlap of these ratios with atmospheric ^{40}Ar/^{36}Ar ratios implies little to no excess ^{40}Ar. Assuming that both dates can be interpreted as the ^{40}Ar/^{39}Ar closure dates of the primary K-feldspar and secondary adularia, Schmieder et al. (2010) interpreted the former date as indicative of the formation age of the RCIS and the latter date as the timing of an episode of hydrothermal activity that persisted for a very short period after the impact.

Paleomagnetics

Initial paleomagnetic studies of the RCIS impactites were done by Pohl and Soffel (1971). They collected samples for all four impactite types, but the Babaudus and Rochechouart were reported as too weakly magnetic for proper analysis. The Montoume and Chassenon samples yielded a combined mean declination of 46.4° and mean inclination of 34.8° (n=130, k=310, α_{95}=4°). They reported that these numbers were indicative of a Late Triassic or Early Jurassic age, and that they were broadly consistent with the initial K/Ar ages for Rochechouart (154-173 Ma), as well the fission track ages for Rochechouart (~200 Ma).

New data from Carpozen and Gilder (2006) seemed to narrow the age constraints for RCIS. In this study, 52 cores were sampled at Rochechouart in a combination of Babaudus, Montoume, and host rock lithologies. For the impact breccias, a total of 25 demagnetized samples from 20 cores yielded a combined mean declination of 35.6° and mean inclination of 42.7° (k=806.9, α_{95}=4.3°) and display both reversed and normal polarities. This places the breccias within an age bracket of 210 to 220 Ma, a narrower margin than that of Pohl and Soffel (1971). While addressing the differences between their data and those of Pohl and Soffel, Carpozen and Gilder asserted that their virtual dipole moment (VPM) is most likely time-averaged due to the slower cooling of the Babaudus and Montoume impactites, whereas the Pohl and Soffel data offer a record of instantaneous VPMs.

The paleomagnetics were readdressed in Eitel et al. (2014). Seventy-two new cores from nine impactite outcrop sites (Montoume, Chassenon, and Valette) were collected. Like those analyzed by Carpozen and Gilder (2006), these impactite samples recorded both reverse and normal polarities, but the new study also identified mixed polarities in some samples, mainly those with the highest percentage of melt. The interpretation of Eitel and co-workers was that the impact most likely occurred during a reversed polarity state (recorded by the Montoume and Chassenon samples) and subsequent self-reversal occurred in the melt-rich samples, causing the observed normal and mixed polarities. Additionally, if it is assumed that the Rochechouart impactites averaged secular variation, the Eitel et al. (2014) results are consistent with the 210 to 220 Ma age picks of Carpozen and Gilder when compared to the European plate apparent polar wander path (APWP). However, Eitel and co-workers assert that if the

impactites did not average secular variation, comparison to the APWP is not appropriate, and the 210-220 Ma age is not necessarily correct.

CHRONOMETERS USED FOR THIS STUDY AND THEIR RECORDS OF SUCCESS IN DATING IMPACT EVENTS

U/Pb

For determining the ages of crystalline igneous rocks on Earth, the ZrnPb method has become the 'gold standard' for accuracy and precision (Schoene 2014). It seems intuitive that the ZrnPb method should be equally valuable for dating impact events, but attempts to use the method for this purpose have had mixed success. To the best of our knowledge, impactites from only four impact structures have been successfully dated by ZrnPb in an unequivocal way: Manicouagan, Vredefort, Morokweng, and Sudbury (Hodych and Dunning 1992; Kamo et al. 1996; Hart et al. 1997; Davis 2008). In all of these cases, the dates – obtained by thermal ionization mass spectrometry (TIMS) –were of very high precision ($2\sigma \leq 0.6\%$). For structures that were also dated by other methods such as $^{40}Ar/^{39}Ar$ or (U-Th)/He, the ZrnPb dates were far more precise (e.g., Jourdan et al. 2009; van Soest et al. 2011). Unfortunately, the list of structures for which ZrnPb has been attempted, but has failed to produce an unambiguous indication of an impact age, is far longer than the list for which the method was an unqualified success.

There are two over-arching reasons why some ZrnPb datasets may be of limited value for impact chronology: 1) the target rocks in most impact structures contained pre-impact zircons; and 2) the U/Pb systematics of those pre-impact zircons appear not to have been reset during the impact event, or to have been only partially reset. The process of isotope chronometer resetting – for ZrnPb as well as a variety of other chronometers

Table 2: Previously published chronological data for the RCIS.

Method	Impactite Analyzed				Other Rock Type		References
	B[a]	M[a]	C[a]	R[a]	PV[a]	BR[a]	
K/Ar	157.7 ± 8.2[b] 177.0 ± 8.2[b] 169 ± 10[b]	--	--	--	--	--	French and Kraut 1971 French and Kraut 1971 Lambert 1974b
Rb/Sr	185.4 ± 8.4	--	--	--	--	--	Reimold and Oskierski 1987
Rb/Sr	--	--	--	--	217 ± 16	--	Reimold et al. 1987
Fission track	--	--	206 ± 39 198 ± 25	--	--	--	Wagner and Storzer 1975 (Gl) Wagner and Storzer 1975 (Ap)
$^{40}Ar/^{39}Ar$	--	--	--	--	214 ± 8	--	Kelley and Spray 1997
$^{40}Ar/^{39}Ar$	--	--	--	--	--	201 ± 2	Schmieder et al. 2010
Paleomagnetics	--	←	UT/LJ →	--	--	--	Pohl and Soffel 1971
Paleomagnetics	← 210-220 →		--	--	--	--	Carpozen and Gilder 2006; Eitel et al. 2014[c]

[a] The impact rock type shorthand descriptions are found in Table 1. Other abbreviations are: PV=pseudotachylite vein, BR=basement rock, Ap=apatite, Gl=glass, UT=Upper Triassic, LJ=Lower Jurassic. All ages are in millions of years and the uncertainties are 2σ, when applicable.
[b] Ages recalculated with Dalrymple (1979) conversion factors that use the updated Steiger and Jäger (1977) K decay constant.
[c] Eitel et al. (2014) agree with these age constraints if the RCIS impactites averaged secular variation.

commonly applied to impact studies –was explored by Young et al. (2013). Based on experimentally derived diffusion parameters for Pb in zircon (Cherniak and Watson 2001) and the mathematics of thermally activated diffusive loss of radiogenic daughter products (Watson and Cherniak 2013), Figure 2 illustrates the combination of durations and maximum temperatures required during an impact event for essentially complete resetting of the ZrnPb chronometer (Young et al. 2013). Also superimposed on this figure are notional ranges of temperatures and timescales for two primary stages of impact structure evolution (contact and compression and excavation) and one secondary impact process (hydrothermal activity). The relationships shown here suggest that only pre-impact zircons in the central target regions of impact craters that experience the highest temperature conditions of the contact and compression stage are likely to have their U/Pb systematics fully reset to the impact age, but they will not be reset during the excavation stage or hydrothermal activity.

The highest probability of successful ZrnPb dating of an impact event is when the event produced a significant amount of impact melt and new zircons – referred to hereafter as "neoblastic zircons" – grew from the melt. In fact, the four successfully dated structures are very large (with crater diameters ≥70 km) and have voluminous crystalline impact melt sheets, and the dated zircons were neoblastic, either as distinctive crystals or as overgrowths on pre-impact crystals. Even in crystalline impact melt sheets, the total zircon populations are likely mixtures of pre-impact and neoblastic zircons, so that isolating and dating neoblastic zircon can be challenging (Armstrong et al. 2002). In this thesis, I illustrate how laser ablation U/Pb dating by inductively coupled, plasma mass spectrometry (LA-ICPMS) may enable the identification of predominately neoblastic

crystals in such mixed populations, such that crystals can be specifically dated by TIMS U/Pb with the highest possible precision.

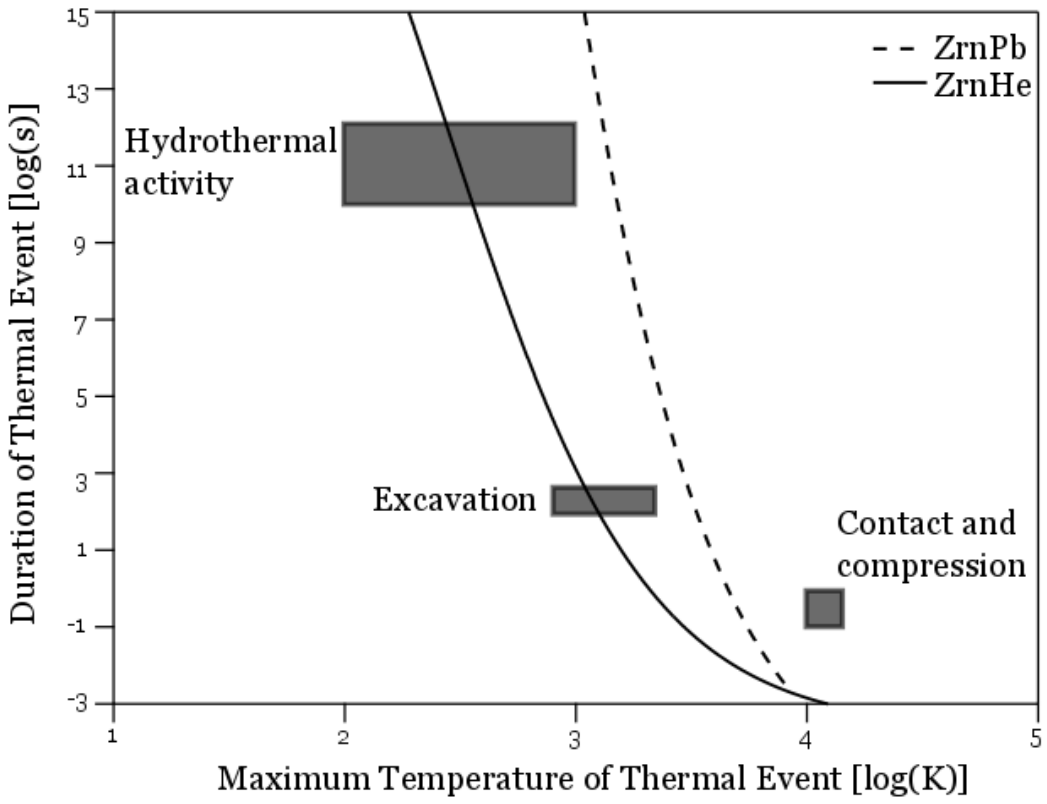

Figure 2: Thresholds for 99% resetting of the U/Pb and (U-Th)/He systematics of pre-impact zircons, after Young et al. (2013). Blue and red curves represent the thresholds for ZrnPb and ZrnHe, respectively. Also shown are notional ranges for temperatures and durations of the stages of impact structure evolution. Sources for these ranges and additional details on how this figure was produced may be found in Young et al. (2013).

(U-Th)/He

Figure 2 also illustrates the equivalent resetting curve for the ZrnHe chronometer. Because all three stages of impact structure development can potentially reset this chronometer, it should be a powerful tool for impact studies, and this has been demonstrated for several structures (Wartho et al. 2009; Peate et al. 2010; van Soest et

al. 2011; Wartho et al. 2012a; Wartho et al. 2012b; Biren et al. 2013; Young et al. 2013; Biren et al. 2014; Young 2014). A typical pattern observed in such studies is that a portion of ZrnHe dates have been totally reset to a young age, but others are only partially reset. This common result is usually interpreted to be related to the fact that the notional temperature-timescale regions for excavation and hydrothermal activity also extend to parts of the graph in Figure 2 that lay below and to the left of the ZrnHe resetting curve and thus in the domain of only partial resetting (Young et al. 2013). If this hypothesis is correct, the youngest mode of ZrnHe dates from an impactite can be reasonably interpreted as the age of impact. However, the same diffusivity characteristics of He in zircon that make ZrnHe an effective chronometer for impact structures also make the chronometer susceptible to post-impact partial or complete resetting during subsequent, regionally significant thermal events (Reiners 2005). As a consequence, the method is most successful when applied to impact structures than show no evidence of significantly post-impact thermal activity, as is the case for the RCIS (Schmieder et al. 2010).

Radiation Damage

All minerals commonly used for U/Pb and (U-Th)/He dating also experience time-dependent structural damage principally as a consequence of α decay, which suggests a chronologic method that has not previously been applied to U+Th-rich minerals in impactites. Radiation damage dating of zircons was initially proposed in the 1950s (Holland and Kulp 1950; Kulp et al. 1952; Hurley and Fairburn 1953). Holland and Gottfried (1955) demonstrated a strong correlation between structural damage in a Sri Lankan zircon, as determined by X-ray diffraction, and its α dose, which is determined by U and Th abundances and a zircon's crystallization age. They suggested that this

correlation could be used to determine radiation damage ages. However, due to the fact that radiation damage anneals over time, especially at elevated temperatures, the notion of radiation damage dating of zircon – a chronometric method we refer to here with the acronym ZrnRD – fell out of favor for the better part of four decades before its revival by Pidgeon and co-workers in the relatively recent past (e.g., Pidgeon et al. 2014).

There are two keys to this revival. The first is conceptual; like ZrnHe or fission track, ZrnRD should be regarded as a thermochronometer, not a geochronometer. As noted by Pidgeon et al. (2014), the current radiation damage in a zircon crystal represents that which has accumulated since the crystal cooled though some relatively narrow temperature range, such that we can think of a ZrnRD closure temperature analogously to how we think about the transition from open to closed system behavior for radiogenic isotopes (Dodson 1973; Hodges 2014). Pidgeon et al. (2014) suggested a notional value of ca. 230˚C for the "closure" temperature of the ZrnRD chronometer. A second key is the more widespread availability of Raman microscopes that enable rapid, non-destructive, quantitative, and high spatial-resolution characterization of structural damage in single zircons (Nasdala et al. 2001; Palenik et al. 2003). In this thesis, we present what is thought to be the first application of this technique to terrestrial impactite dating.

SAMPLE SELECTION

Samples of the Montoume and Babaudus impactites were collected in July and August of 2015 for this project. These units were selected for sampling because they typically contain higher percentages of melt than other RCIS impactites (Sapers et al. 2014). After examination, the four Montoume samples showing the least amount of

obvious alteration (RIC_15_002, RIC_15_005, RIC_15_014, and RIC_15_015) and one relatively unaltered Babaudus sample (RIC_15_013) were selected for characterization and chronology. Collection localities are shown in Figure 1.

Montoume Sample Characteristics

Samples RIC_15_002 and RIC_15_005 were collected in-situ, while RIC_15_014 and RIC_15_015 were pieces of float found at the Montoume quarry. This material is characteristically red on both weathered and fresh surfaces. With the exception of RIC_15_002, the Montoume impactite samples are best classified as clast-rich impact melt breccias, with a quartzofeldspathic devitrified matrix cement. Clasts were found to be both monomineralic quartz and polymineralic (quartz + K-feldspar) lithic fragments, with sizes ranging from sub-millimeter to several decimeters. Many clasts and quartz crystals display shock features, including: 1) planar deformation features in quartz, which appear as a network of intersecting, intracrystal lines indicative of mechanical failure planes (Whitehead et al. 2002); 2) toasted quartz, which appears as lightly brown, nonpleochroic crystals and is thought to be indicative of submicron fluid inclusions (Whitehead et al. 2002); and 3) ballen features, which appear as intracrystal, spheroidal to ellipsoidal fractures that can indicate recrystallized diaplectic quartz glass that transitioned from cristobalite back to α-quartz (Ferrière et al. 2009). In comparison, RIC_15_002 was finer grained and notably clast-poor (Figure 3). Most clasts in RIC_15_002 are shocked quartz xenocrysts with a grain size of less than 1 mm, although a few rare clasts between 1 and 2 mm were observed. Clasts in all samples were angular to sub-angular.

A polished thin section prepared from RIC_15_002 was studied in some detail by backscattered electron (BSE) imaging and energy-dispersive spectrometry (EDS) to

elucidate mineralogy and general matrix composition using a JEOL JXA-8530F electron microprobe at Arizona State University's John M. Cowley Center for High Resolution Electron Microscopy. For both BSE and EDS, the microprobe was operated at 15 kV and ranged between 40 and 80 nA for varied acquisition times.

Figure 3: Hand sample photos of clast-poor (RIC_15_002, left) and clast-rich (RIC_15_015, right) samples of Montoume impactite.

In thin section, RIC_15_002 reveals itself to be an impact melt rock with elongated vesicles at microscale; this elongation is interpreted as a flow feature, similar to flow features also observed in hand specimen. Unlike in the Babaudus sample (described below), the vesicles are not filled with secondary mineralization. The matrix of this rock is essentially fully devitrified into a quartz+feldspar aggregate with titanium-rich biotite and Fe-Ti oxide as accessory minerals (Figure 4). The small clasts in the impactite acted as nucleation centers around which devitrified glass recrystallized in radial bundles of feldspar (Figure 5). The matrix largely consists of quartz and K-feldspar. An important difference between RIC_15_002 and the other studied Montoume samples is that it contains a small percentage of biotite. This biotite appears as subhedral crystals with long dimensions in thin section of up to 1-2 mm. Accessory Fe-

Ti oxides occur as both rounded (several tens of micrometers) and elongated grains (long axis: 20 to 150 micrometers) and can contain small inclusions of quartz.

RIC_15_015, representing the clast-rich Montoume samples, was also studied in thin section. While unfilled vesicles are not as common in the clast-rich samples as they are in the clast-poor sample, elongated microscale-vesicles can be observed in the RIC_15_015 thin section. Similarly to RIC_15_002, this sample has a fine-grained,

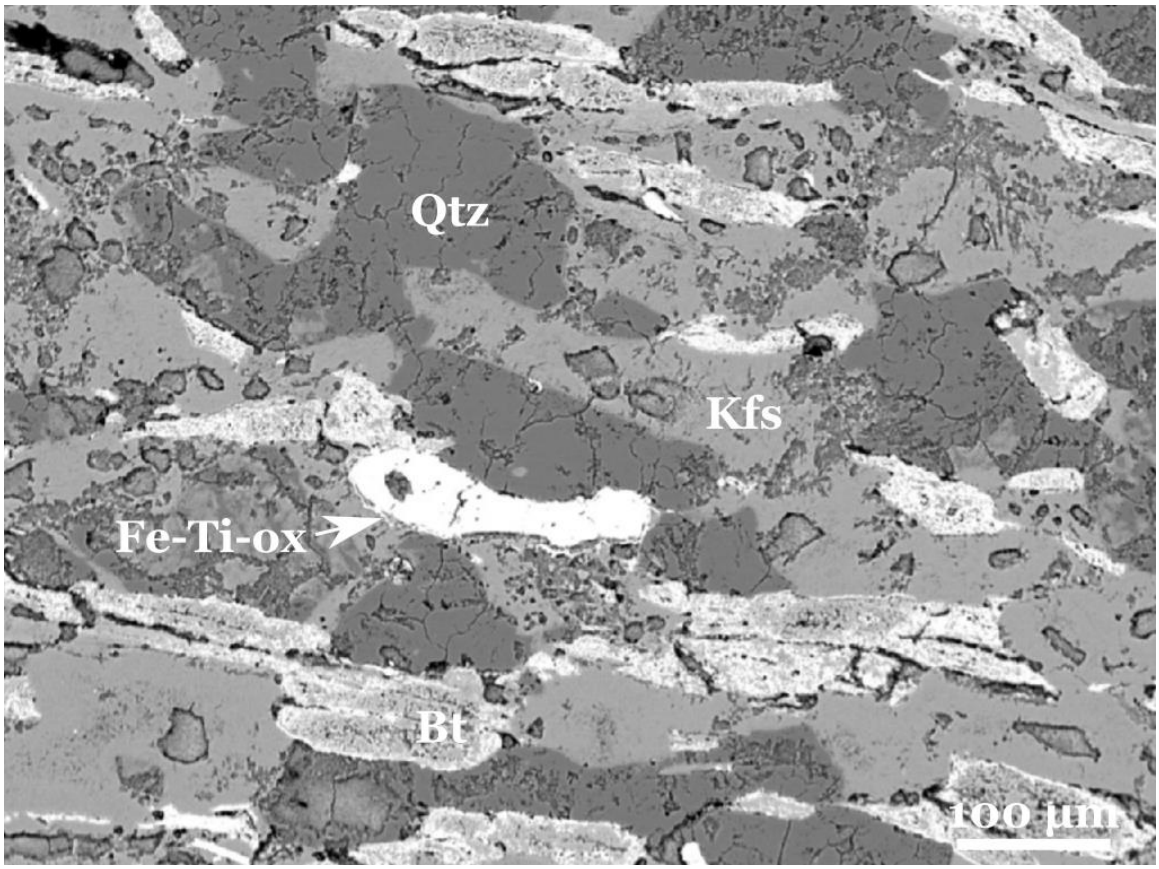

Figure 4: BSE image of the main and accessory minerals of sample RIC_15_002. Abbreviations are: Qtz=quartz, Kfs=K-feldspar, Fe-Ti-ox=Fe-Ti oxide, Bt=biotite.

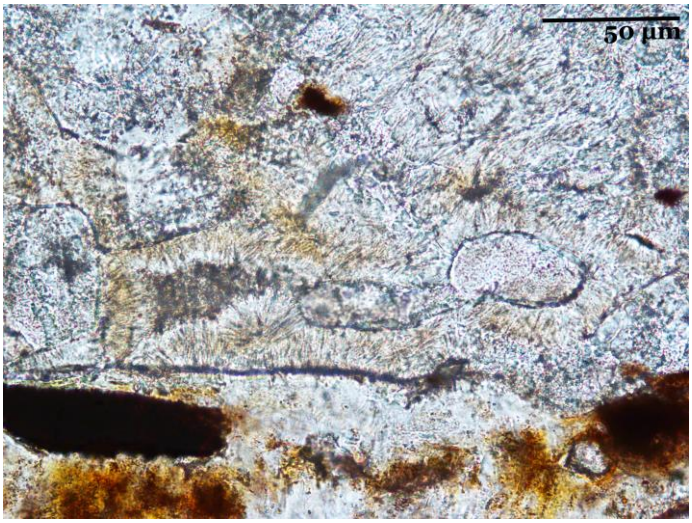

Figure 5: Laths of feldspar growing radially from clasts in RIC_15_002, PPL.

quartzofeldspathic matrix, with accessory Fe-Ti oxides similar to those described in RIC_15_002. Although the groundmass mineralogy is similar as well, the radial overgrowths around clasts are less common in the clast-rich samples, and the matrix seems less devitrified. Under the microscope, shock features are obvious in both monomineralic quartz clasts and the quartz within lithic clasts.

Babaudus Sample Characteristics

The Babaudus impactite is best described as a clast-poor impact melt rock. Representative sample RIC_15_013 has an appearance strikingly different from the Montoume impactite, displaying a buff-colored matrix with easily distinguished, similarly colored lithic clasts on a fresh surface. Weathered surfaces of the impactite appear dark gray, black, or dark yellow. The clasts range in size from less than a millimeter to several centimeters. Many of these lithic clasts show evidence of partial assimilation in the melt, while monomineralic quartz xenocrysts in the rock show little evidence of assimilation. Shock features found in clasts of the Montoume impactite are also common in the lithic clasts and quartz xenocrysts in this sample.

Petrographic, BSE, and EDS reconnaissance study of a thin section of RIC_15_013 reveals it to be more vesicular than any of the studied Montoume samples. Amygdaloidal, iron-rich chlorite typically lines or entirely fills the vesicles; it most likely represents post-impact hydrothermal alteration and/or near-surface weathering (Figure 6, French and Kraut 1971; Sapers et al. 2014). Based on EDS observations, the most prevalent mineral presently in the 'melt' matrix of this sample is recrystallized orthoclase, although small (5-10 μm) crystals of pyroxene and quartz were identified as well. The matrix of this sample contains less quartz than the RIC_15_002 section of the Montoume impactite. In plane-polarized light (PPL), pervasive iron-oxide staining is observed, a product of post-impact hydrothermal alteration (Sapers et al. 2014). Unlike the Montoume samples, there are no observed Fe-Ti oxides in RIC_15_013, however Sapers et al. (2014) reported submicron Fe-Ti oxides in the Babaudus sample from their study.

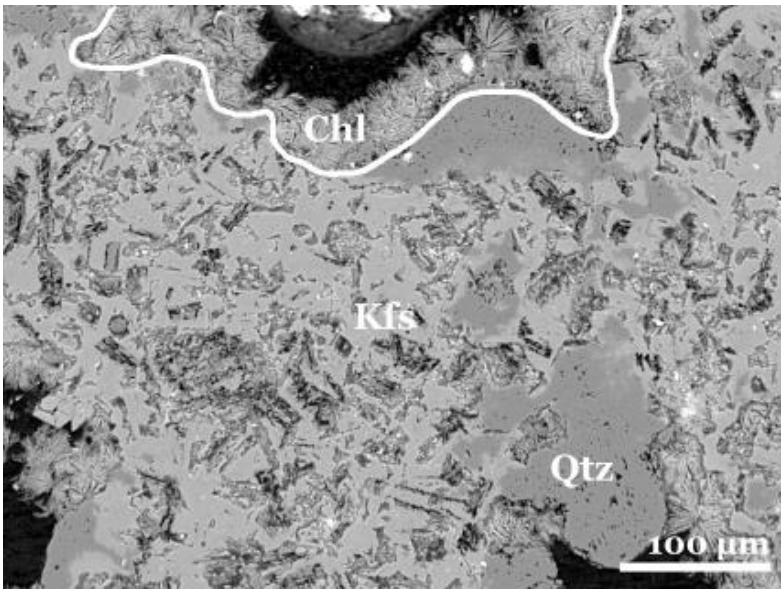

Figure 6: BSE image of a portion of the melt matrix of Babaudus sample RIC_15_013. The white line delineates a vesicle partially filled with iron-rich chlorite. Abbreviations are: Chl=chlorite, Kfs=K-feldspar, Qtz=quartz.

ANALYTICAL METHODS

ZrnHe Chronometry

ZrnHe dates were determined for 9 zircons in Babaudus sample RIC_15_013 and 10, 10, 10, and 6 zircons in Montoume samples RIC_15_002, RIC_15_005, RIC_15_014, and RIC_15_015, respectively. Zircons were separated in bulk using magnetic and gravimetric techniques, and individual zircons – euhedral, free of obvious inclusions and fractures, and with grain sizes ≥ 50 μm – were selected for (U-Th)/He analysis. These zircons were measured and encapsulated in Nb tubes for analysis in the Group 18 Laboratories at Arizona State University. Helium analysis was done using an Australian Scientific Instruments *Alphachron MkII* system, with gasses extracted by heating with an infrared (970 nm) diode laser. Re-extracts continued for each zircon until ^{4}He output was less than 0.5% of the initial extraction. Samples were then dissolved using standard procedures (see Appendix A) and parent isotopes (^{238}U, ^{232}Th) analyzed by inductively coupled, plasma source mass spectrometry (ICP-MS) with a Thermo Scientific *i-Cap Q* instrument. ^{235}U abundance is calculated from the analyzed ^{238}U, using the widely accepted Steiger and Jäger (1977) ^{238}U/^{235}U value of 137.88. ^{147}Sm typically contributes <1% to ^{4}He production and is not a commonly occurring trace element in zircon, and thus was not analyzed for this study. Analytical procedures were monitored by ZrnHe analyses of individual crystals of the Fish Canyon zircon standard (Horne et al. 2016); two standards were analyzed for every twenty RCIS impactite analyses. Alpha ejection correction factors were calculated based on the method of Hourigan et al. (2005).

ZrnPb Chronometry

ZrnPb dates were generated for 37 zircons in Babaudus sample RIC_15_013 and 43, 47, 37, and 27 zircons in Montoume samples RIC_15_002, RIC_15_005,

RIC_15_014, and RIC_15_015, respectively, by laser ablation ICPMS (LA-ICPMS) in the Group 18 Laboratories. One batch of hand-picked, ≥ 50 μm, and inclusion-free zircons from all samples were mounted in *TorrSeal* (a low vapor-pressure, UHV adhesive), while a second batch of hand-picked, ≥ 20 μm, and inclusion-free zircons were mounted in epoxy. After polishing, the grain mounts were loaded into a Photon Machines *HelEx* dual volume ablation cell for material extraction by ablation using a Photon Machines *Analyte G2* ArF excimer ultraviolet (193 nm) laser. Laser energy was applied at 5 mJ (100% output power) with a pulse frequency of 5 Hz for 100-400 seconds to produce ablation pit sizes ranging from 25 to 65 μm in diameter and with depths of 10-35 μm. Ablated material was streamed to the plasma source of a Thermo Scientific *i-Cap Q* quadrupole mass spectrometer for analysis using a He carrier gas. Prior to sample analysis, the mass spectrometer was auto-tuned using National Institute of Standards and Technology (NIST) 612 glass, and system performance was monitored by an analysis of Plešovice zircon standard (Sláma et al. 2008) after each five unknown analyses. Data reduction was performed using the *Iolite* software procedural package for *Igor Pro*.

Radiation Damage Chronometry

Because the radiation damage dating method may be less familiar to readers than (U-Th)/He or U/Pb, we provide a more detailed description of our ZrnRD procedures here. The essential equation describing the development of α radiation damage (D_α) over time in a zircon is:

$$D_\alpha = 8 * \left(\frac{C_U * N_A * 0.9928}{M_{238} * 10^6}\right) * \left(e^{\lambda_{238} t} - 1\right) + 7 * \left(\frac{C_U * N_A * 0.0072}{M_{235} * 10^6}\right) * \left(e^{\lambda_{235} t} - 1\right)$$
$$+6 * \left(\frac{C_{Th} * N_A}{M_{232} * 10^6}\right) * \left(e^{\lambda_{232} t} - 1\right) \quad (1)$$

where C_U and C_{Th} are the concentrations of U and Th in the zircon; M_{232} , M_{235} , and M_{238} are the molecular weights of ^{232}Th, ^{235}U, and ^{238}U; λ_{232} , λ_{235} , and λ_{238} are the decay

constants of ^{232}Th, ^{235}U, and ^{238}U; N_A is Avogadro's number; and t is the elapsed time (Nasdala et al. 2001). Given U and Th analyses and a knowledge of the amount of radiation damage in a zircon, a ZrnRD date can be calculated iteratively from Equation 1, solving for t.

For our study, ZrnRD dates were determined for 15 zircons in Babaudus sample RIC_15_013 and 11, 19, 13, and 2 zircons in Montoume samples RIC_15_002, RIC_15_005, RIC_15_014, and RIC_15_015, respectively. Hand-picked ≥ 50 μm and inclusion-free zircons from these samples were mounted in TorrSeal and polished prior to spectral analysis using a HORIBA Scientific XploRA PLUS confocal Raman microscope in the Group 18 Laboratories. Of special interest for our application is the finding by Palenik et al. (2003) that the full width at half maximum of the ~1010 cm^{-1} v_3 (SiO_4) Raman band for zircon (hereafter $FWHM_{SiO4}$) correlates with D_α as defined in Equation 1. For each zircon, we used the Raman microscope to measure $FWHM_{SiO4}$ at a central position on its polished surface using a focused visible (532 nm) laser and a 2,400 gr/mm grating, with variable filtering (between 50% and 100%) and acquisition time (between 5 and 30 s) to maximize signal/background ratios. During analysis, the footprint of the laser was ca. 2 μm. After corrections of the measured $FWHM_{SiO4}$ based on the spectral resolution of the Raman microscope (Irmer 1985), we assigned the resulting value a nominal 1σ of 5%, following Pidgeon et al. (2014). We then used the empirical correlation relationship between $FWHM_{SiO4}$ and D_α suggested by Palenik et al. (2003) to arrive at an input value for Equation 1.

After the Raman measurements, the polished sample was loaded into the Photon Machines *HelEx* cell for laser ablation U and Th analyses using the same procedures as described above for ZrnPb analyses. The resulting U and Th values thus average over a

much larger domain of zircon than the domain sampled by Raman analysis. Uncertainties for ZrnRD dates were estimated using a Monte Carlo error propagation routine that accounts for uncertainties in the FWHM measurement, in parameters of the conversion relationship of Palenik et al. (2003), and in U and Th concentration measurements.

CHRONOLOGICAL RESULTS AND INTERPRETATIONS

A summary of my best interpretations of the age of the RCIS based on application of the ZrnHe, ZrnPb, and ZrnRD chronometers is presented in Table 3. All of the data is documented in Appendix B as tables (e.g., Table S1 for the ZrnHe data). All new ZrnHe, ZrnPb, and ZrnRD dates in the tables and the text of this thesis are reported at the 95% confidence level, which is close to – but slightly different from – the 2σ level.

ZrnHe

ZrnHe dates for the Babaudus sample ranged from 142.7 ± 4.0 Ma to 283.9 ± 8.6 Ma (Table S1). Similar variations were found for each of the Montoume samples; collectively, the ZrnHe dates for all Montoume zircons ranged from 109.3 ± 3.2 Ma to 270.5 ± 3.9 Ma. The dates for each sample are overdispersed, which is to say that they scatter more than would be anticipated from analytical imprecision alone. There are many potential causes for overdispersion in ZrnHe data (as reviewed by Hodges and Mercer, manuscript in preparation; Hourigan et al. 2005), but a major factor in impactites is incomplete resetting of the (U-Th)/He chronometer in pre-impact zircons during transient impact events (Young et al. 2013). In many cases, this manifests as a frequency distribution of dates – depicted either using the summed probability density plot or a kernel density estimator plot (Vermeesch 2012) – that is highly skewed,

Table 3. ZrnHe, ZrnPb, and ZrnRD Results from This Study.

Chronometer	Mean (Ma)	N[a]	Impactite(s)[b]
ZrnHe	191.6 ± 9.1[c]	39	M+B
ZrnPb	202.6 ± 5.8[c]	8	M
ZrnRD	211 ± 13[c]	8	M+B

[a] Number of zircon analyses included in the mean.

[b] Descriptions of the Montoume (M) and Babaudus (B) impactites included in text and Table 1.

[c] ZrnHe mean does not include the six outliers discussed in text. All errors reported at the 95% confidence level.

with a preponderance of young ZrnHe dates (interpreted as roughly corresponding to the impact age) and a 'tail' of older ZrnHe dates that reflect target rocks thermally unaffected by the impact. There is no clear evidence of such a pattern in our RCIS ZrnHe data (Figure 7); in fact, the data illustrate a broadly symmetric pattern dispersed about a single mode, as is shown particularly by the kernel density plot for all 45 Montoume and Babaudus zircons. The implication of this is that the (U-Th)/He systematics of these zircons were nearly completely reset during impact, and any partial resetting is masked by large amounts of dispersion due to other factors, such as U-Th zoning. It is also possible that the very young (Cretaceous) ZrnHe dates reflect post-impact ^{4}He loss related to a previously unrecognized post-impact alteration event.

Given the observed distribution in (Figure 7), our best estimate for the ZrnHe age of the impact event corresponds roughly to the maxima of the kernel density estimator plot in Figure 7, and might be computed explicitly as the inverse-variance weighted mean of ZrnHe dates from all samples. For all 45 zircons, the result is 177.93 ± 0.82 Ma with an MSWD of 193.5. This extremely high MSWD reflects extreme overdispersion of the data and suggests that it would be appropriate to examine the dataset for obvious outliers that might be excluded for the calculation of the mean. Unfortunately, there are

no obvious unusual characteristics of specific zircons (such as inclusions or subhedral habit) that might argue for exclusion, so we are left to using statistical methods in our search for outliers. We elected to use a modified version of the Hampel outlier method (Davies and Gather 1993; Pearson 2011) in which we take into consideration the specific uncertainties of each ZrnHe date (Hodges and Mercer, manuscript in preparation). Using the Hodges and Mercer approach, which assumes a conservative Hampel outlier limit of 4, the modified Hampel identifier method identified six outliers (Table S1), and a recalculation of the inverse-variance weighted mean of the remaining 39 zircons yields 191.64 ± 0.95 Ma. The MSWD for this mean is much better than that for all 45 points (91.9 *vs.* 193.5), but still reflects major overdispersion. It is very common in the geochronology community to assign a more robust uncertainty to a calculated inverse-variance weighted mean for overdispersed data by multiplying the formal uncertainty by the square-root of the MSWD (Ludwig 1991; York et al. 2004). Doing so results in our preferred (but highly imprecise) ZrnHe age for the RCIS impact of 191.6 ± 9.1 Ma (Table 3).

In order for this ZrnHe age to adequately define the impact event, two criteria must be met: 1) the analyzed impactites had to cool and become a closed system with regards to He loss within a geologically insignificant time period after impact; and 2) no post-impact thermal event disturbed the (U-Th)/He systematics. Although the impact-induced hydrothermal alteration at the RCIS caused elevated temperatures to persist post-impact, studies of other similarly-sized impact structures suggest that impact-related hydrothermal activity is typically short-lived. For example, hydrothermal activity associated with the 24 km Haughton crater in Canada persisted only a few tens of thousands of years after collision (Osinski et al. 2001), while hydrothermally altered

impactites from the 23 km Ries crater, Germany, are thought to have cooled from 600°C to 100°C within 2,000 years after collision (Pohl et al. 1977). These examples indicate that the first criterion was likely met. The question of whether the second criterion is met is a little more ambiguous. There is no reported post-impact magmatic or metamorphic event in this region (Schmieder et al. 2010); however, it is possible there was an as-of-yet unrecognized post-impact thermal event, which is indicated by the small population of young ZrnHe dates and the partial fading in fission tracks observed by Wagner and Storzer (1975). Despite this possibility, we interpret the ZrnHe date as broadly indicative of the age of the Rochechouart-Chassenon impact event.

ZrnPb

Due to variable degrees of common Pb contamination in the RCIS zircons selected for dating, we define their ZrnPb dates here as $^{206}Pb/^{238}U$ dates, which are less affected by unintentionally improper common Pb corrections. The ZrnPb dates for all 191 dated zircons (Table S2) display a strongly skewed distribution with a broad Phanerozoic maxima and a tail that extends to the Paleoproterozoic (Figure 8). Except for one clear outlier in the RIC_15_005 dataset (denoted in Table S2), the youngest ZrnPb dates are Late Triassic or Early Jurassic. There is only moderate variation in the median ZrnPb dates among the Montoume and Babaudus samples (357 to 430 Ma). Overall, in light of previous geochronologic work in the region, we interpret the distribution of dates to indicate the presence of: 1) pre-Variscan zircons which are likely detrital grains derived from the metasedimentary rocks of the Massif Central; 2) Variscan zircons of igneous and possibly metamorphic origin; and 3) post-Variscan zircons associated with late-orogenic or post-orogenic magmatism (Alexandrov et al. 2000; Alexandre 2007; Melleton et al. 2010). Of particular interest is the presence of a few crystals of apparently

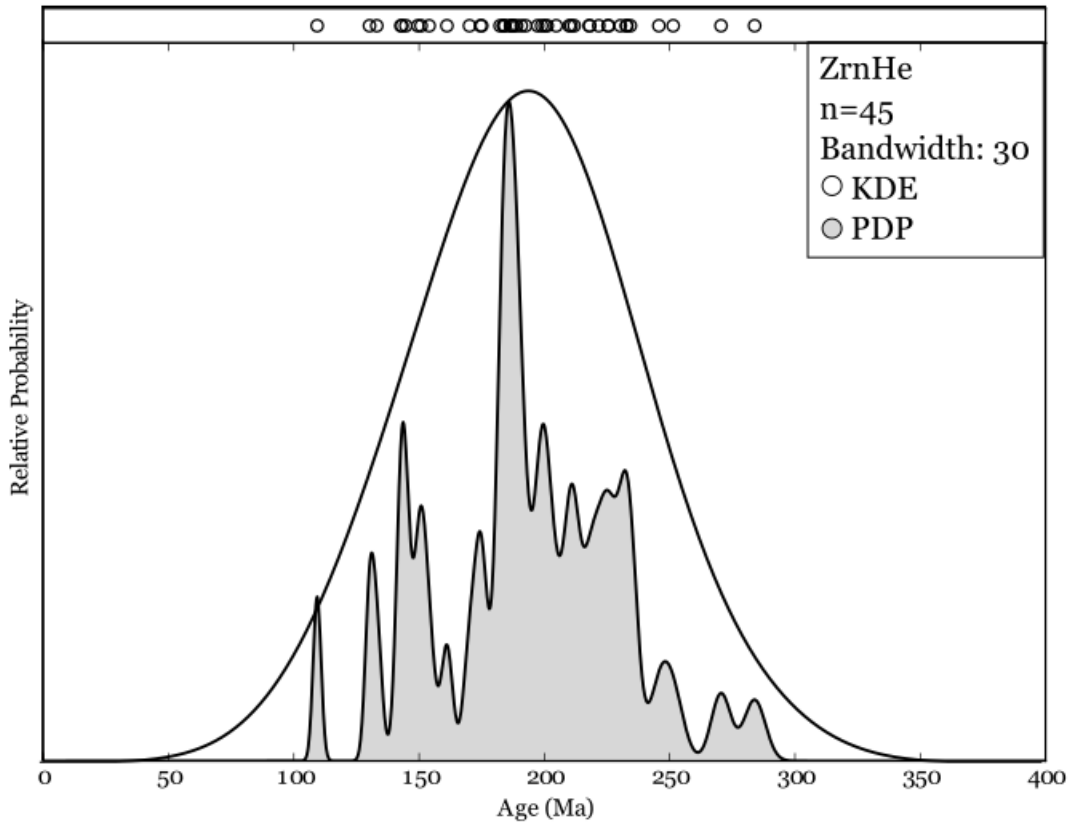

Figure 7: Probability density (gray) and kernel density estimator (unfilled) plots for the ZrnHe dataset. Small open circles indicate specific dates. Kernel density estimator was calculated assuming a bandwidth of 30. Data are in Table S1, Appendix B.

neoblastic (impact-related) zircon in every sample except RIC_15_013 (the Babaudus impactite), comprising a subpopulation of n = 8 crystals in all. These zircons yield an inverse variance-weighed mean date of 202.6 ± 1.6 Ma with an MSWD of 12.5. The dispersion of these dates, while limited compared to that encountered for the RCIS ZrnHe dates, is still more than anticipated on the basis of analytical uncertainties alone. To some extent, this may reflect post-impact alteration or potentially the possibility that the grains contain neoblastic zircon overgrowths on pre-impact zircons. Our analytical protocols did not permit the kind of high spatial-resolution $^{206}Pb/^{238}U$ analyses (which might be possible using an ion microprobe) that would be necessary to address such

questions. For now, we conservatively multiply the analytically derived uncertainty by the square root of the MSWD to arrive at what we regard as the best available ZrnPb age of the RCIS at the 95% confidence level: 202.6 ± 5.8 Ma (Figure 8).

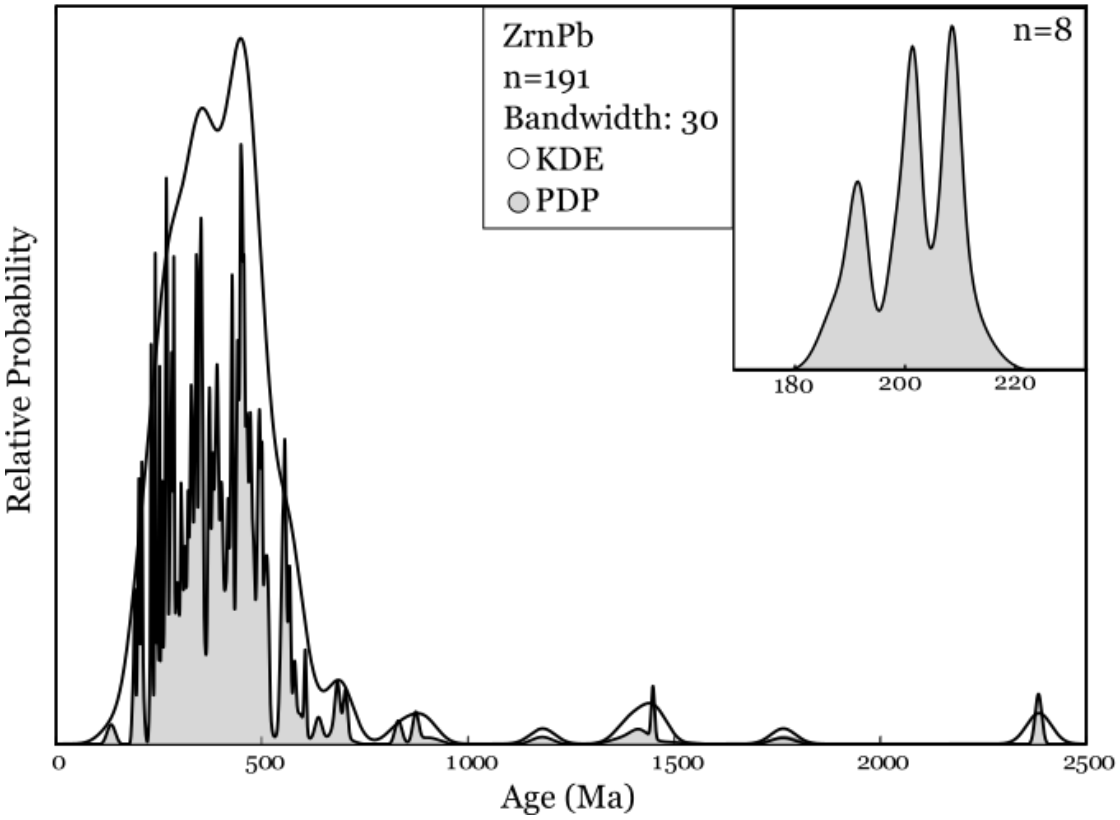

Figure 8: Probability density (gray) and kernel density estimator (unfilled) plots for the ZrnPb dataset. Kernel density estimator was calculated assuming a bandwidth of 30. Data are in Table S2, Appendix B. The inset depicts the PDP (gray) of the eight youngest zircon grains (excluding the RIC_15_005 outlier), which we interpret as neoblastic zircons.

ZrnRD

Radiation damage dates for the RCIS samples (Table S3) have larger notional uncertainties (ca. 7% at 1σ) than either ZrnPb or ZrnHe dates. Much of this can be attributed to propagated uncertainties of the Palenik et al. (2003) fitting parameters used to relate $FWHM_{SiO4}$ to D_α. Despite these larger uncertainties, the ZrnRD dates are

highly overdispersed, both for individual samples and for the entire set of 60 dates (Figure 9). They range from a low of 108 ± 16 Ma to a high of 1050 ± 130 Ma. We hypothesize that at least some of this dispersion is related to U+Th zoning in the zircon. While our laser ablation analytical procedure for U and Th averages across relatively large volumes of zircon by design, our single-spot surface Raman measurements with a narrow beam footprint do not average across domains of different U+Th concentration and thus D_α. Nevertheless, we regard most of the observed dispersion in ZrnRD dates to be an indication of incomplete annealing of pre-impact irradiation damage in many of the analyzed zircons.

Figure 9 shows the same sort of strongly skewed distribution as the ZrnPb dataset depicted in Figure 8. Disregarding the outlying ZrnRD dates >800 Ma, the distribution in Figure 9 shows two prominent modes at ca. 210 and ca. 470 Ma. Notably, the latter is consistent with significant ZrnPb populations in the Massif Central gneisses that characterized the target for RCIS (e.g., Melleton et al. 2010). We infer that the young mode represents radiation damage dates for neoblastic zircons crystallized from the impact melt and pre-impact zircons that were completely reset by the RCIS event. This mode is defined by eight zircons, six of which were separated from Montoume impactite sample RIC_15_005. The inverse variance-weighted mean ZrnRD date for these zircons is 211 ± 13 Ma at the 95% confidence level, which agrees with both the ZrnHe and ZrnPb impact ages. The MSWD of this mean – 0.28 – is better than might be anticipated from the presumed analytical uncertainties, plausibly indicating that our assignments of uncertainties for ZrnRD data are overly pessimistic.

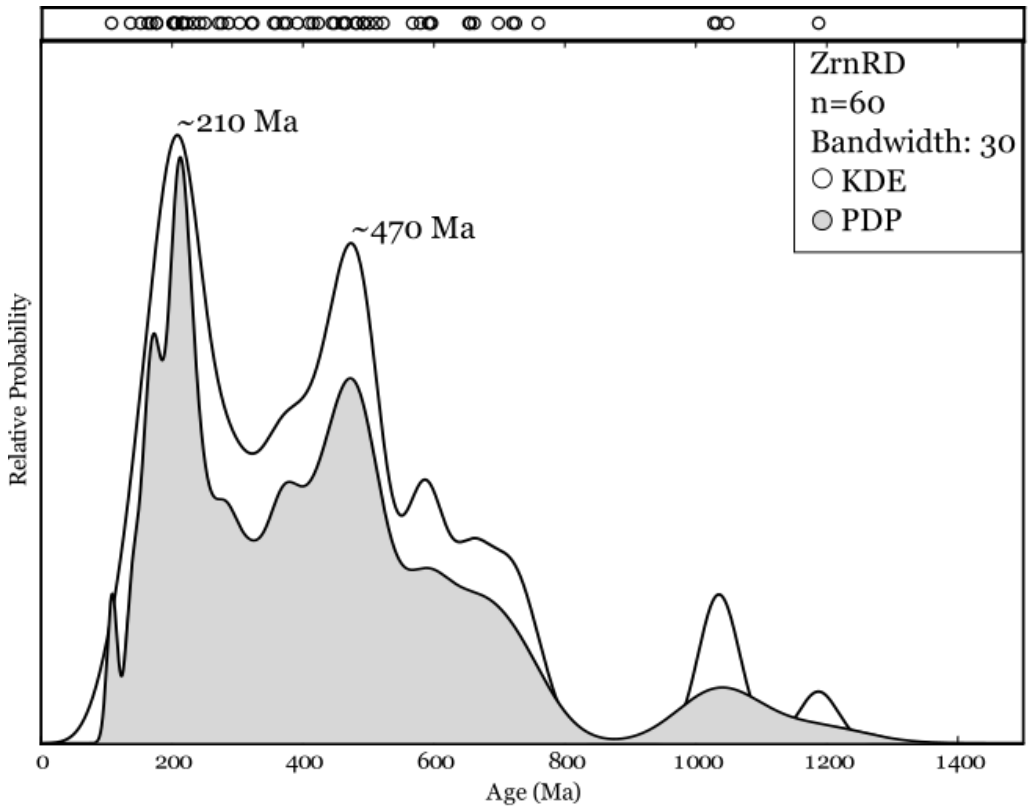

Figure 9: Probability density (gray) and kernel density estimator (unfilled) plots for the ZrnRD dataset. Small open circles indicate specific dates. Kernel density estimator was calculated assuming a bandwidth of 30. Data are in Table S3, Appendix B.

Discussion

We conclude that this study's ZrnHe, ZrnPb, and ZrnRD mean dates of 191.6 ± 9.1 Ma, 202.6 ± 5.8 Ma, and 211 ± 13 Ma are dating the true impact age, and display a clear agreement with the Schmieder et al. (2010) 201 ± 2 Ma (2σ) $^{40}Ar/^{39}Ar$ age, suggesting RCIS should be excluded from the Spray et al. (1998) Late Triassic Multiple Impact Event. It also suggests the impactites at Rochechouart did not average secular variation, as suggested in Eitel et al. (2014). Although less precise than the $^{40}Ar/^{39}Ar$ data, these chronometers successfully resolved the discrepancy between Schmieder et al. (2010) and Kelley and Spray (1997). It is important to remember that high precision is

not always synonymous with accuracy; the multichronometric approach provides a method to check the accuracy of various datasets.

The ZrnPb results are important to this study because this chronometer is typically unaffected by low-temperature thermal events that may reset the ZrnHe chronometer (Figure 2). The ZrnPb chronometer can remain undisturbed through metamorphic events, sedimentary processes, and magmatic entrainment (e.g. Pankhurst and Pidgeon 1976; Harrison et al. 1987; Riggs et al. 1996; Cherniak and Watson 2001). We regard the ZrnPb impact age as a moderately precise indication of the Rochechouart-Chassenon impact event, however it is highly likely that the ~2.8% precision could be improved by using a TIMS for analyses. This brings to light an interesting method for obtaining highly precise impact ages. The laser ablation ICP-MS technique is a relatively simple and time-efficient process – it can analyze a large number of zircons in a short amount of time. For impact craters with relatively small volumes of melt sheet, LA-ICP-MS can provide a 'pre-TIMS reconnaissance' on a large number of zircons and potentially identify a small subset of impact-aged zircons. These grains can be extracted from the mount and subsequent TIMS U/Pb analysis could provide a more precise age for the impact.

Although the ZrnRD data provide interesting and supportive information, the low precision makes it difficult to confidently draw conclusions from this chronometer alone. Rochechouart is the first impact crater this method was applied to, but it is relatively small and contains only a small percentage of recrystallized zircons in its melt rocks, as evidenced by the U/Pb data. Applying the ZrnRD chronometer to a larger crater with an extensive melt sheet would most likely lower the dispersion; it would be interesting to

compare the results from this study and, for instance, ZrnRD data from Manicouagan, where the presence of newly grown zircons are more abundant.

Paleogeographic and tectonic reconstructions for the Late Triassic indicate that the Rochechouart-Chassenon impact occurred in shallow waters of the Tethys Sea (Ziegler et al. 1983; Ziegler 1988; Lambert 2010). The Massif Central may have been one of many small islands off the northern Gondwana margin that were separated by shallow channels of water (Ziegler 1988). The present-day British Isles occupied a similar paleogeographic position. Simms (2003) reported severe soft sediment deformation in siltstones and sandstones of the Cotham Member (Lilstock Formation, Penarth Group, Rhaetian) in the United Kingdom that he interpreted as a 1-4 m-thick seismite, overlain by a discontinuous, ≤1 m-thick tsunamite deposit. The observed lateral extent (~250,000 km^2) is anomalously large for a seismite and is difficult to explain through conventional terrestrial processes, like earthquakes or volcanic eruptions (Simms 2003, 2007). Even the most intense earthquakes (M>9) typically disturb rocks or sediments <500 km from the epicenter (Obermeier 1996). Given that the observed lateral extent is the minimum region affected—there is no Cotham Member outcrop in the UK that lacks a ≥1 m seismite—Simms (2003) asserted that an impact is the most likely cause for these observed deposits, considering the necessary high-energy nature of the event.

Although there are no reported distal ejecta found in this area, the timing of the seismite deposit overlaps with the likely Rochechouart-Chassenon impact age based on our data and those of Schmieder et al. (2010). The seismite is underlain by mudstones of the Rhaetian Westbury Formation, providing an upper age limit of ~208.5 Ma (IUGS Chronostratigraphic Chart, 2013). Within 1 to 13 m above the seismite, the ammonite *Psiloceras* appears in mudstones and limestones of the Lias Group; the appearance of

this fossil presently characterizes the boundary between the Triassic and Jurassic (Hodges 1994). This implies a lower age limit of ~201 Ma for the seismite (IUGS Chronostratigraphic Chart, 2013). Simms (2003) asserted that the seismite was deposited no more than ~1 million years before the end-Triassic extinction, but due to the undisturbed sediments between the top of the seismite formation and the appearance of *Psiloceras*, it is unlikely the end-Triassic extinction and seismites are correlated.

CONCLUSIONS

Zircons from the Montoume and Babaudus impactites at the Rochechouart-Chassenon impact structure yield (U-Th)/He, U/Pb, and radiation damage dates that are all consistent with the previously published Schmieder et al. (2010) $^{40}Ar/^{39}Ar$ date of 201 ± 2 Ma for impact-affected target materials. The most precise of our constraints are from a sub-population of eight apparently neoblastic zircons yielding an inverse variance-weighted mean ZrnPb date of 202.6 ± 5.8 Ma. We regard it as probable that the imprecision of this date relates to the analytical methodology used and that thermal ionization mass spectrometry (TIMS) dating of neoblastic zircons from the RCIS (in progress) will likely yield the highest precision and most robust estimate of the timing of impact. ZrnHe dates for the impactites are overdispersed but yield a weighted mean date of 191.6 ± 9.1 Ma (n=39).

This is the first study to attempt to use radiation damage as an absolute dating method for impactites. Our radiation damage dates are imprecise compared to those obtained using isotopic chronometers and highly dispersed, but they display two major populations at ca. 210 Ma and ca. 470 Ma. We interpret the former population as

including zircons that were nearly completely annealed in the impact event; their inverse-variance weighted mean date of 211 ± 13 Ma (n=8) is consistent with the isotopic data.

The statistical consistency of U/Pb, $^{40}Ar/^{39}Ar$, (U-Th)/He, and radiation damage geochronological data reported here and in Schmieder et al. (2010) strongly support the interpretation that the Rochechouart-Chassenon impact took place within uncertainty of the Triassic-Jurassic boundary, not as part of an earlier impact catena as suggested by Spray et al. (1998). While it seems highly unlikely that the Rochechouart-Chassenon impact was related in any significant way to the nearly simultaneous, globally significant, end-Triassic biologic extinction event (Blackburn et al. 2013), possible regional affects may have included seismite and tsunamite deposits in the present-day British Isles (Simms 2003).

REFERENCES CITED

Aldrich, L. T., and G. W. Wetherill. "Geochronology by radioactive decay." *Annual Review of Nuclear Science* 8, no. 1 (1958): 257-298.

Alexandre, P. "U–Pb zircon SIMS ages from the French Massif Central and implication for the pre-Variscan tectonic evolution in Western Europe." *Comptes Rendus Geoscience* 339, no. 9 (2007): 613-621.

Alexandrov, P, A.Cheilletz, É. Deloule, and M. Cuney."319±7 Ma crystallization age for the Blond granite (northwest Limousin, French Massif Central) obtained by U/Pb ion-probe dating of zircons." *Earth and Planetary Science* 330, no. 9 (2000): 617-622.

Alvarez, L. W., W. Alvarez, F. Asaro, and H. V. Michel. "Extraterrestrial cause for the Cretaceous-Tertiary extinction: Experiment and theory." (1980): 1095-1108.

Armstrong, R., S. Vishnevsky, and C. Koeberl. "U-Pb Analyses of Zircons from the Popigai Impact Structure, Russia: First Results." In *Impacts in Precambrian Shields*, pp. 109-116. Springer Berlin Heidelberg, 2002.

Blackburn, T. J., P. E. Olsen, S. A. Bowring, N. M. McLean, D. V. Kent, J. Puffer, G. McHone, E. T. Rasbury, and M. Et-Touhami. "Zircon U-Pb geochronology links the end-Triassic extinction with the Central Atlantic Magmatic Province." *Science* 340, no. 6135 (2013): 941-945.

Biren, M. B., M. C. van Soest, J-A. Wartho, and J. G. Spray. "(U-Th)/He Dating of Uplift-Induced Cooling in a Complex Terrestrial Impact Structure: The Manicouagan Example." *Meteoritics and Planetary Science Supplement* 75 (2013): 5344.

Biren, M.B., M. C. van Soest, J.-A. Wartho, and J. G. Spray. "Dating the cooling of exhumed central uplifts of impact structures by the (U–Th)/He method: A case study at Manicouagan." *Chemical Geology* 377 (2014): 56-71.

Carporzen, L., and S. A. Gilder. "Evidence for coeval Late Triassic terrestrial impacts from the Rochechouart (France) meteorite crater." *Geophysical research letters* 33, no. 19 (2006).

Cherniak, D. J., W. A. Lanford, and F. J. Ryerson. "Lead diffusion in apatite and zircon using ion implantation and Rutherford backscattering techniques." *Geochimica et Cosmochimica Acta* 55, no. 6 (1991): 1663-1673.

Cherniak, D. J., and E. B. Watson. "Pb diffusion in zircon." *Chemical Geology* 172, no. 1 (2001): 5-24.

Dalrymple, G. B. "Critical tables for conversion of K-Ar ages from old to new constants." *Geology* 7, no. 11 (1979): 558-560.

Davies, L., and U. Gather. "The identification of multiple outliers." *Journal of the American Statistical Association* 88, no. 423 (1993): 782-792.

Davis, D. W. "Sub-million-year age resolution of Precambrian igneous events by thermal extraction–thermal ionization mass spectrometer Pb dating of zircon: Application to crystallization of the Sudbury impact melt sheet." *Geology* 36, no. 5 (2008): 383-386.

Dence, M. R. "A comparative structural and petrographic study of probable Canadian meteorite craters." *Meteoritics* 2, no. 3 (1964): 249-270.

Dodson, M. H. "Closure temperature in cooling geochronological and petrological systems." *Contributions to Mineralogy and Petrology* 40, no. 3 (1973): 259-274.

Douce, A. E. P. "Titanium substitution in biotite: an empirical model with applications to thermometry, O_2 and H_2O barometries, and consequences for biotite stability." *Chemical Geology* 108, no. 1 (1993): 133-162.

Duthou, J. L., J.M. Cantagrel, J. Didier, and Y. Vialette. "Paleozoic granitoids from the French Massif Central: age and origin studied by 87 Rb□ 87 Sr system." *Physics of the Earth and Planetary Interiors* 35, no. 1 (1984): 131-144.

Eitel, M., S. A. Gilder, T. Kunzmann, and J. Pohl. "Rochechouart impact crater melt breccias record no geomagnetic field reversal." *Earth and Planetary Science Letters* 387 (2014): 97-106.

Farley, K. A. "(U-Th)/He dating: Techniques, calibrations, and applications." *Reviews in Mineralogy and Geochemistry* 47, no. 1 (2002): 819-844.

Farley, K. A., R. A. Wolf, and L. T. Silver. "The effects of long alpha-stopping distances on (U-Th)/He ages." *Geochimica et Cosmochimica Acta* 60, no. 21 (1996): 4223-4229.

Faure, M., E. B. Mézème, M. Duguet, C. Cartier, and J.-Y. Talbot. "Paleozoic tectonic evolution of medio-Europa from the example of the French Massif Central and Massif Armoricain." *Journal of the Virtual Explorer* 19, no. 5 (2005): 1-25.

Faure, M., E. B. Mézème, A. Cocherie, P. Rossi, A. Chemenda, and D. Boutelier. "Devonian geodynamic evolution of the Variscan Belt, insights from the French Massif Central and Massif Armoricain." *Tectonics* 27, no. 2 (2008).

Ferrière, L., C. Koeberl, and W. U. Reimold. "Characterisation of ballen quartz and cristobalite in impact breccias: new observations and constraints on ballen formation." *European Journal of Mineralogy* 21, no. 1 (2009): 203-217.

Harrison, T. M., J. N. Aleinikoff, and W. Compston. "Observations and controls on the occurrence of inherited zircon in Concord-type granitoids, New Hampshire." *Geochimica et Cosmochimica Acta* 51, no. 9 (1987): 2549-2558.

Hart, R. J., M.A. G. Andreoli, M. Tredoux, D. Moser, L. D. Ashwal, E. A. Eide, S. J. Webb, and D. Brandt. "Late Jurassic age for the Morokweng impact structure, southern Africa." *Earth and Planetary Science Letters* 147, no. 1 (1997): 25-35.

Hildebrand, A. R., G. T. Penfield, D. A. Kring, M. Pilkington, A. Camargo, S. B. Jacobsen, and W. V. Boynton. "Chicxulub crater: a possible Cretaceous/Tertiary boundary impact crater on the Yucatan Peninsula, Mexico." *Geology* 19, no. 9 (1991): 867-871.

Hodges, K. V. "Thermochronology in Orogenic Systems." In *Treatise on Geochemistry* 4, Second Edition, edited by H.D. Holland and K.K. Turekian, 281-308. Elsevier, Oxford (2014).

Hodges, P. "The base of the Jurassic System: new data on the first appearance of Psiloceras planorbis in southwest Britain." *Geological Magazine* 131, no. 06 (1994): 841-844.

Hodych, J. P., and G. R. Dunning. "Did the Manicouagan impact trigger end-of-Triassic mass extinction?" *Geology* 20, no. 1 (1992): 51-54.

Holland, H. D., and D. Gottfried. "The effect of nuclear radiation on the structure of zircon." *Acta Crystallographica* 8, no. 6 (1955): 291-300.

Holland, H. D., and J. L. Kulp. "Geologic age from metamict minerals." *Science* 111, no. 2882 (1950): 312-312.

Horn, W., and A. El Goresy. "The Rochechouart Crater in France: Stony and not an Iron Meteorite?" In *Lunar and Planetary Science Conference*, vol. 11, pp. 468-470. 1980.

Horn, W., and A. El Goresy. "Discovery of metallic residues of the Rochechouart meteorite in basement rocks." *Bulletin de Mineralogie* 104, no. 4 (1981): 587-593.

Horne, A. M., M. C. van Soest, K. V. Hodges, A. Tripathy-Lang, and J. K. Hourigan. "Integrated single crystal laser ablation U/Pb and (U–Th)/He dating of detrital accessory minerals–Proof-of-concept studies of titanites and zircons from the Fish Canyon tuff." *Geochimica et Cosmochimica Acta* 178 (2016): 106-123.

Hourigan, J. K., P. W. Reiners, and M. T. Brandon. "U-Th zonation-dependent alpha-ejection in (U-Th)/He chronometry." *Geochimica et Cosmochimica Acta* 69, no. 13 (2005): 3349-3365.

Hurley, P. M., and H.W. Fairbairn. "Radiation damage in zircon: a possible age method." *Geological Society of America Bulletin* 64, no. 6 (1953): 659-673.

Irmer, G. "On the influence of the apparatus function on the determination of scattering cross sections and lifetimes from optical phonon spectra." *Experimentelle Technik der Physik* 33 (1985): 501-506.

Janssens, M.-J., J. Hertogen, H. Takahashi, E. Anders, and P. Lambert. "Rochechouart meteorite crater: Identification of projectile." *Journal of Geophysical Research* 82, no. 5 (1977): 750-758.

Jourdan, Fred, P. R. Renne, and W. U. Reimold. "An appraisal of the ages of terrestrial impact structures." *Earth and Planetary Science Letters* 286, no. 1 (2009): 1-13.

Kamo, S. L., W. U. Reimold, T. E. Krogh, and W. P. Colliston. "A 2.023 Ga age for the Vredefort impact event and a first report of shock metamorphosed zircons in pseudotachylitic breccias and granophyre." *Earth and Planetary Science Letters* 144, no. 3 (1996): 369-387.

Kelley, S. P., and J. G. Spray. "A late Triassic age for the Rochechouart impact structure, France." *Meteoritics & Planetary Science*32, no. 5 (1997): 629-636.

Koeberl, C., A. Shukolyukov, and G. W. Lugmair. "Chromium isotopic studies of terrestrial impact craters: Identification of meteoritic components at Bosumtwi, Clearwater East, Lappajärvi, and Rochechouart." *Earth and Planetary Science Letters* 256, no. 3 (2007): 534-546.

Kraut, F. "Sur l'origine des clivages du quartz dans les brèches 'volcaniques' de la région de Rochechouart." C. R. H. Acad. Sci., Ser. D 264, no. 23 (1967): 2609.

Kraut, F. "A new impact occurrence in the area of Rochechouart-Chassenon (Haute Vienne et Charente, France)." *Geologica Bavarica* 61 (1969): 428-450.

Kraut, F., and B. M. French. "The Rochechouart meteorite impact structure, France: Preliminary geological results." *Journal of Geophysical Research* 76, no. 23 (1971): 5407-5413.

Krogh, T. E., D. W. Davis, and F. Corfu. "Precise U-Pb zircon and baddeleyite ages for the Sudbury area." In *The Geology and Ore Deposits of the Sudbury Structure*, vol. 1, pp. 431-446. Ontario: Ontario Geological Survey, 1984.

Kulp, J. L., H. L. Volchok, and H. D. Holland. "Age from metamict minerals." *American Mineralogist (US)* 37 (1952).

Lambert, P. "Etude géologique de la structure impactitique de Rochechouart (Limousin, France) et son contexte." *Bull. BRGM Sec. I* 3 (1974a): 153-164.

Lambert, P. “La Structure d’Impact de Météorite Géante de Rochechouart.” PhD diss., Paris-Sud Université, 1974b: 55-56.

Lambert, P. "Rochechouart impact crater-Statistical geochemical investigations and meteoritic contamination." In *Impact and Explosion Cratering: Planetary and Terrestrial Implications (*eds. D. J. Roddy, R. O. Pepin and R. B. Merrill), pp. 449-460. 1977.

Lambert, P. "The Rochechouart crater: Shock zoning study." *Earth and Planetary Science Letters* 35, no. 2 (1977): 258-268.

Lambert, P. "Target and impact deposits at Rochechouart impact structure, France." *Geological Society of America Special Papers* 465 (2010): 509-541.

Lippolt, H. J., and E. Weigel. "^{4}He diffusion in ^{40}Ar-retentive minerals." *Geochimica et Cosmochimica Acta* 52, no. 6 (1988): 1449-1458.

Lippolt, H. J., M. Leitz, R. S. Wernicke, and B. Hagedorn. "(Uranium+ thorium)/helium dating of apatite: experience with samples from different geochemical environments." *Chemical Geology* 112, no. 1 (1994): 179-191.

Lippolt, H. J., R. S. Wernicke, and R. Ba. "Paragenetic specularite and adularia (Elba, Italy): concordant (U+ Th)-He and K-Ar ages." *Earth and Planetary Science Letters* 132, no. 1 (1995): 43-51.

Ludwig, K. R. "Isoplot—A plotting and regression program for radiogenic-isotope data; version 2.53." *U.S. Geological Survey Open File Report* (1991): 91-445.

Melleton, J., A. Cocherie, M. Faure, and P. Rossi. "Precambrian protoliths and Early Paleozoic magmatism in the French Massif Central: U–Pb data and the North Gondwana connection in the west European Variscan belt." *Gondwana Research* 17, no. 1 (2010): 13-25.

Melosh, H. J. *Impact Cratering: A Geologic Process*. New York: Oxford University Press, 1989.

Nasdala, L., M. Wenzel, G. Vavra, G. Irmer, T. Wenzel, and B. Kober. "Metamictisation of natural zircon: accumulation versus thermal annealing of radioactivity-induced damage." *Contributions to Mineralogy and Petrology* 141, no. 2 (2001): 125-144.

Nasdala, L., J. M. Hanchar, A. Kronz, and M. J. Whitehouse. "Long-term stability of alpha particle damage in natural zircon." *Chemical Geology* 220, no. 1 (2005): 83-103.

Nier, A. O. "A redetermination of the relative abundances of the isotopes of carbon, nitrogen, oxygen, argon, and potassium." *Physical Review* 77, no. 6 (1950): 789.

Norman, M. D., and A. A. Nemchin. "A 4.2 billion year old impact basin on the Moon: U–Pb dating of zirconolite and apatite in lunar melt rock 67955." *Earth and Planetary Science Letters* 388 (2014): 387-398.

Obermeier, S. F. "Use of liquefaction-induced features for paleoseismic analysis—an overview of how seismic liquefaction features can be distinguished from other features and how their regional distribution and properties of source sediment can be used to infer the location and strength of Holocene paleo-earthquakes." *Engineering Geology* 44, no. 1 (1996): 1-76.

Orton, G., K. Baines, D. Deming, and M. A. Hearn. "Collision of comet Shoemaker-Levy 9 with Jupiter observed by the NASA infrared telescope facility." *Science* 267, no. 5202 (1995): 1277.

Osinski, G. R., J. G. Spray, and P. LEE. "Impact-induced hydrothermal activity within the Haughton impact structure, arctic Canada: Generation of a transient, warm, wet oasis." *Meteoritics & Planetary Science*36, no. 5 (2001): 731-745.

Palenik, C. S., L. Nasdala, and R. C. Ewing. "Radiation damage in zircon." *American Mineralogist* 88, no. 5-6 (2003): 770-781.

Palme, H., M.-J. Janssens, H. Takahashi, E. Anders, and J. Hertogen. "Meteoritic material at five large impact craters." *Geochimica et Cosmochimica Acta* 42, no. 3 (1978): 313-323.

Pankhurst, R. J., and R. T. Pidgeon. "Inherited isotope systems and the source region pre-history of early Caledonian granites in the Dalradian Series of Scotland." *Earth and Planetary Science Letters* 31, no. 1 (1976): 55-68.

Pearson, R. *Exploring data in engineering, the sciences, and medicine*. New York: Oxford University Press, 2011.

Pidgeon, R. T. "Zircon radiation damage ages." *Chemical Geology* 367 (2014): 13-22.

Pohl, J., and H. Soffel. "Paleomagnetic age determination of the Rochechouart impact structure (France)." *Z. Geophys* 37 (1971): 857-866.

Pohl, J., D. Stöffler, H. Gall, and K. Ernstson. "The Ries impact crater." In *Impact and explosion cratering: Planetary and terrestrial implications*, pp. 343-404. 1977.

Reimold, W. U., L. Bischoff, J. Nieber-Reimold, W. Oskierski, and A. Rehfeldt. "Petrographic and geochemical studies on the basement rocks of the Rochechouart meteorite crater, France, and pseudotachylite therein." In *Lunar and Planetary Science Conference*, vol. 14, pp. 636-637. 1983.

Reimold, W. U., W. Oskierski, and H. Schafer. "The Rochechouart impact melt: Geochemical implications and Rb-Sr chronology." In *Lunar and Planetary Science Conference*, vol. 15, pp. 685-686. 1984.

Reimold, W. U., W. Oskierski, and J. Huth. "The pseudotachylite from Champagnac in the Rochechouart meteorite crater, France." *Journal of Geophysical Research: Solid Earth* 92, no. B4 (1987a). 7

Reimold, W. U., and W. Oskierski. "The Rb-Sr-age of the Rochechouart impact structure, France, and geochemical constraints on impact melt-target rock-meteorite compositions." In *Research in terrestrial impact structures*, pp. 94-114. Vieweg + Teubner Verlag. 1987b.

Reimold, W. U., H. Leroux, and R. L. Gibson. "Shocked and thermally metamorphosed zircon from the Vredefort impact structure, South Africa." *European Journal of Mineralogy* 14, no. 5 (2002): 859-868.

Riggs, N. R., T. M. Lehman, G. E. Gehrels, and W. R. Dickinson. "Detrital zircon link between headwaters and terminus of the Upper Triassic Chinle-Dockum paleoriver system." *Science* 273, no. 5271 (1996): 97.

Sapers, H. M., G. R. Osinski, N. R. Banerjee, L. Ferrière, P. Lambert, and M. R. M. Izawa. "Revisiting the Rochechouart impact structure, France." *Meteoritics & Planetary Science* 49, no. 12 (2014): 2152-2168.

Schmieder, M., E. Buchner, W. H. Schwarz, M. Trieloff, and P. Lambert. "A Triassic/Jurassic Boundary Age for the Rochechouart Impact Structure (France)." *Meteoritics and Planetary Science Supplement* 72 (2009): 5138.

Schoene, B. "U–Th–Pb Geochronology." In *Treatise on Geochemistry* 4, Second Edition, edited by H.D. Holland and K.K. Turekian, 341-378. Elsevier, Oxford (2014).

Schulte, P., L. Alegret, I. Arenillas, J. A. Arz, P. J. Barton, P. R. Bown, T. J. Bralower et al. "The Chicxulub asteroid impact and mass extinction at the Cretaceous-Paleogene boundary." *Science* 327, no. 5970 (2010): 1214-1218.

Simms, M. J. "Uniquely extensive seismite from the latest Triassic of the United Kingdom: Evidence for bolide impact?" *Geology* 31, no. 6 (2003): 557-560.

Simms, M. J. "Uniquely extensive soft-sediment deformation in the Rhaetian of the UK: Evidence for earthquake or impact?" *Palaeogeography, Palaeoclimatology, Palaeoecology* 244, no. 1 (2007): 407-423.

Sláma, J., J. Košler, D. J. Condon, J. L. Crowley, A. Gerdes, J. M. Hanchar, M. S. A. Horstwood, G. A. Morris, L. Nasdala, N. Norberg, U. Schaltegger, B. Schoene, M. N. Tubrett, and M. J. Whitehouse. "Plešovice zircon—a new natural reference material for U–Pb and Hf isotopic microanalysis." *Chemical Geology* 249, no. 1 (2008): 1-35.

Spray, J. G., S. P. Kelley, and D. B. Rowley. "Evidence for a late Triassic multiple impact event on Earth." *Nature* 392, no. 6672 (1998): 171-173.

Steiger, R. H., and E. Jäger. "Subcommission on geochronology: convention on the use of decay constants in geo-and cosmochronology." *Earth and planetary science letters* 36, no. 3 (1977): 359-362.

Strutt, R. “On the radio-active minerals.” *Proc. Roy. Soc. London* 76 (1905): 88-101.

Tagle, R., R. T. Schmitt, and J. Erzinger. "Identification of the projectile component in the impact structures Rochechouart, France and Sääksjärvi, Finland: Implications for the impactor population for the earth." *Geochimica et Cosmochimica Acta* 73, no. 16 (2009): 4891-4906.

Ukstins Peate, I., M. C. van Soest, J-A. Wartho, N. Cabrol, E. Grin, J. Piatek, J. Piatek, and G. Chong. "A novel application of (U-Th)/He geochronology to constrain the age of small, young meteorite impact craters: A case study of the Monturaqui crater, Chile." In *Lunar and Planetary Science Conference*, vol. 41, p. 2161. 2010.

Van Soest, M. C., K. V. Hodges, J.-A. Wartho, M. B. Biren, B. D. Monteleone, J. Ramezani, J. G. Spray, and L. M. Thompson. "(U-Th)/He dating of terrestrial impact structures: The Manicouagan example." *Geochemistry, Geophysics, Geosystems* 12, no. 5 (2011).

Vermeesch, P. "On the visualisation of detrital age distributions." *Chemical Geology* 312 (2012): 190-194.

Wagner, G. A., and D. Storzer. "The age of the Rochechouart impact structure." *Meteoritics* 10 (1975): 503.

Wartho, J-A., M. Schmieder, M. C. Van Soest, E. Buchner, K. V. Hodges, R. K. Bezys, and W. U. Reimold. "New (U-Th)/He Zircon and Apatite Ages for the Lake Saint Martin Impact Structure (Manitoba, Canada) and Implications for the Late Triassic Multiple Impact Theory." In *Lunar and Planetary Science Conference*, vol. 40, p. 2004. 2009.

Wartho, J-A., M. C. van Soest, F. J. Cooper, J. G. Spray, M. Schmieder, E. Buchner, D. T. King et al. "(U-Th)/He Dating of Impact Structures-The Big, the Small, and the Potential Limitations." *Meteoritics and Planetary Science Supplement* 75 (2012a): 5279.

Wartho, J.-A., M. C. van Soest, D. T. King, and L. W. Petruny. "An (U-

Th)/He age for the shallow-marine Wetumpka impact structure, Alabama, USA." *Meteoritics & Planetary Science* 47, no. 8 (2012b): 1243-1255.

Watson, E. B., and D. J. Cherniak. "Simple equations for diffusion in response to heating." *Chemical Geology* 335 (2013): 93-104.

Weaver, H. A., C. Arpigny, D. C. Boice, and M. F. A. Hearn. "The Hubble Space Telescope (HST) observing campaign on comet Shoemaker-Levy 9."*Science* 267, no. 5202 (1995): 1282.

Wendt, I., and C. Carl. "The statistical distribution of the mean squared weighted deviation." *Chemical Geology: Isotope Geoscience Section* 86, no. 4 (1991): 275-285.

Whitehead, J., J. G. Spray, and R. A. F. Grieve. "Origin of "toasted" quartz in terrestrial impact structures." *Geology* 30, no. 5 (2002): 431-434.

Wolf, R. A., K. A. Farley, and L. T. Silver. "Helium diffusion and low-temperature thermochronometry of apatite." *Geochimica et Cosmochimica Acta* 60, no. 21 (1996): 4231-4240.

Yamada, R., T. Tagami, S. Nishimura, and H. Ito. "Annealing kinetics of fission tracks in zircon: an experimental study." *Chemical Geology* 122, no. 1 (1995): 249-258.

York, D., Norman M. E., M. López Martınez, and J. De Basabe Delgado. "Unified equations for the slope, intercept, and standard errors of the best straight line." *American Journal of Physics* 72, no. 3 (2004): 367-375.

Young, K. E., M. C. Soest, K. V. Hodges, E. B. Watson, B. A. Adams, and P. Lee. "Impact thermochronology and the age of Haughton impact structure, Canada." *Geophysical Research Letters* 40, no. 15 (2013): 3836-3840.

Young, K. E. "The Use of Terrestrial Analogs in Preparing for Planetary Surface Exploration: Sampling and Radioisotopic Dating of Impactites and Deployment of In Situ Analytical Technologies." PhD diss., Arizona State University, 2014.

Zeitler, P. K., A. L. Herczeg, I. McDougall, and M. Honda. "U-Th-He dating of apatite: A potential thermochronometer." *Geochimica et Cosmochimica Acta*51, no. 10 (1987): 2865-2868.

Zhang, A.-C., W.-B. Hsu, X.-H. Li, H.-L. Ming, Q.-L. Li, Y. Liu, and G.-Q. Tang. "Impact melting of lunar meteorite Dhofar 458: Evidence from polycrystalline texture and decomposition of zircon." *Meteoritics & Planetary Science* 46, no. 1 (2011): 103-115.

Ziegler, P. A. "Evolution of the Arctic-North Atlantic and the Western Tethys—A

Visual Presentation of a Series of Paleogeographic-Paleotectonic Maps.” *AAPG memoir* 43 (1988): 164-196.

Ziegler, A. M., C. R. Scotese, and S. F. Barrett. "Mesozoic and Cenozoic paleogeographic maps, Tidal friction and the Earth's rotation II P. Brosche, J. Sundermann, 240–252." (1983).

APPENDIX A
ANALYTICAL PROCEDURE IN DETAIL

Zircon Separation

Samples were rock-sawed, hand-crushed, and dry-sieved into three size fractions: >1.4 mm, 0.5-1.4 mm, and <0.5 mm. The latter fraction was wet-sieved into three additional size fractions: 250-500 μm, 120-250 μm, and 50-120 μm. The three size fractions were magnetically separated individually on a Frantz Separator in a 0.2→0.4→0.7→1.0→1.2 A sequence. The yielded materials were subsequently combined due to the small output and the >1.2 A grains were separated by density using lithium heteropolytungstates (LST) heavy liquid. The denser grains were obtained and cleaned in a sonicator, using a liquid sequence of water→ethanol→methanol→acetone, each stage lasting for ten minutes. Once dry, grains were poured into a glass dish and hand-picked.

Mounting: TorrSeal

Double sided tape was flattened onto a glass slide and zircon grains were placed on the tape under a microscope within a one centimeter diameter plastic ring. The TorrSeal mixer gun was given a new tip and the mixture pressed into the ring, using a straight edge to flatten the top (while attempting to minimize bubbles). The glass slide was then placed on a hotplate at 60°C for one hour; temperature was verified by a thermocouple and stayed within 5°C of intended value. The temperature was lowered to 40°C for two hours and then the glass plate removed from the hotplate. The mount was not touched for 72 hours, allowing the TorrSeal to fully cure. It was then extracted from the plastic ring and polished using 30/12/9/3/1/0.5 μm Precision Surfaces International, Inc., MicroAbrasive sheets with water. It was finally sonicated in water for 10 minutes and set out to dry, ready for analysis.

Mounting: Epoxy

Double sided tape was flattened onto a plastic block and zircon grains were placed on the tape under a microscope within a one inch diameter plastic ring. Struers' EpoFix epoxy was mixed using instructions on the box (15:2 volume ratio of resin:hardener) and poured into the plastic ring. The plastic box was placed into a small vacuum system for ~1 hour and then set to cure for 12 hours. The mount was extracted from the plastic ring and very lightly polished using 9/3/1/0.5 μm polishing paper, mainly to rid the mount of tape residue. It was then ready for analysis.

Analysis: Conventional (U-Th)/He

All analyses were completed at Arizona State University's Group 18 Laboratories, supervised by Dr. Kip Hodges.

The zircon grains were loaded into Nb tubes after necessary measurements (perpendicular half-widths, total length, and pyramidal terminations, all found in Table S1), crimped, placed into the Australian Scientific Instruments *Alphachron* palette, and pumped to ultrahigh vacuum (typically accomplished overnight). Two FCT zircon age standards, one Durango fluorapatite shard, and two Nb tube blanks were included for every 20 unknown analyses. The samples were heated with a 45 Watt, 923 nm diode laser and the resulting gas was spiked with ^{3}He and cleaned of reactive gases on a hot getter. Cleaned aliquots were analyzed on a quadrupole mass spectrometer connected to an electron multiplier detector. Between each sample analysis, an aliquot of known ^{4}He was spiked with ^{3}He and analyzed to allow the ^{4}He in unknown sample to be calculated. Samples are re-extracted until the blank-corrected ^{4}He is ≤0.5% of the original output. Average blank was ~0.04 fentomoles of ^{4}He.

Once ^{4}He measurements are complete, samples are unloaded and dissolved for U and Th analysis. Nb tubes are placed in small Teflon tubes and undergo a sequence of:

1) Spike of known U/Th concentration added to all samples
    a. For every 14 unknown samples, one spike standard is prepared
2) Add HF to vials
3) Parr bomb at 225°C for 72 hours
4) Dry down on hotplate
5) Add HCl to vials
6) Parr bomb at 200°C for 24 hours
7) Dry down on hotplate
8) Add HF and HNO_3 to vials
9) Transfer liquid to 15 mL tubes filled with 1.5 mL DI water

Samples are then analyzed on a Thermo Scientific *i-Cap Q* inductively coupled plasma mass spectrometer. Post-analysis, all elements (^{4}He, ^{238}U, ^{232}Th) were blank corrected. ^{235}U was not analyzed, but the widely accepted Steiger and Jaeger 1977 $^{238}U/^{235}U$ ratio of 137.88 approximated its contribution. Uncorrected ages were found iteratively via the fundamental equation:

$$4He = 8 * {}^{238}U * \left(e^{\lambda_{238}t} - 1\right) + 7 * {}^{235}U * \left(e^{\lambda_{235}t} - 1\right) + 6 * {}^{232}Th * (e^{\lambda_{232}t} - 1)$$

^{147}Sm typically contributes <1% to ^{4}He production and was not included in the analysis. These ages were then corrected for alpha ejection using the set of equations initially outlined in Farley et al. (1996) and expanded in Hourigan (2005); the tetragonal prism with pyramidal termination A1/A2 values were used from Hourigan (2005). Errors were propagated through the calculations, but no error was assigned to the alpha ejection correction factor.

Analysis: Laser Ablation U-Pb

Zircon mounts were loaded into a Photon Machines Analyte G2 with a 193 nm excimer laser and HelEx dual volume ablation cell connected to a Thermo Scientific *i-Cap Q* ICP-MS (epoxy and TorrSeal mounts analyzed separately). ICP-MS was auto-tuned while ablating on National Institute of Standards and Technology (NIST) 612 glass. Laser operated at 100% power at 5 mJ and pit sizes ranged from 25 to 65 μm. Plešovice acted as an age standard and one aliquot was analyzed for every 5 unknown grains. Post-analysis, the data was reduced in *Igor Pro* software. Pre-ablation baselines for every pit were fitted and subtracted. The duration of each run was manually refined after importation in the software and the Plešovice standard was designated as the reference material.

APPENDIX B
SUPPLEMENTARY TABLES

Table S1: ZrnHe data for each sample analyzed in this study.

Sample	^{4}He[a]	^{238}U[a]	^{232}Th[a]	$Date_{RAW}$[b]	$2\sigma_{RAW}$[b]	R1[c]	R2[c]	L[c]	H1[c]	H2[c]	B[d]	F_T[e]	$Date_{corr}$[f]	$2\sigma_{corr}$[f]
	10^{11} atoms	10^{11} atoms	10^{11} atoms	Ma	Ma	µm	µm	µm	µm	µm	μm^{-1}	Mean	Ma	Ma
RIC_15_002 (Montoume)														
z1	2.043	9.112	5.518	150.5	4.4	25.1	31.6	118.4	31.9	25.7	0.090	0.64	**234.3**	**6.8**
z2	3.383	16.26	5.147	148.2	4.4	39.2	43.1	161.5	41.7	40.3	0.063	0.75	**198.9**	**5.9**
z3	3.179	17.05	5.883	132.3	3.8	39.9	37.3	126.4	30.9	30.8	0.069	0.72	**183.6**	**5.3**
z4	1.566	8.556	2.916	130.0	3.9	34.8	26.9	130.0	30.1	22.5	0.082	0.68	**192.5**	**5.7**
z5	0.4467	2.529	0.791	126.2	4.1	26.4	27.3	106.9	26.9	24.9	0.095	0.63	**201.1**	**6.6**
z6	0.6185	3.609	1.032	123.2	3.8	30.7	29.2	101.4	25.0	22.5	0.088	0.65	**188.9**	**5.8**
z7	1.331	5.565	3.990	157.0	4.7	30.7	32.2	133.3	36.0	34.0	0.081	0.68	**232.7**	**7.0**
z8	1.017	6.032	2.330	118.7	3.6	26.7	28.7	118.5	25.9	24.3	0.090	0.65	**183.8**	**5.6**
z9	0.849	5.100	2.040	116.9	3.6	29.1	24.9	104.1	25.5	26.6	0.096	0.62	**187.3**	**5.7**
z10	2.798	13.86	8.216	136.0	3.9	39.2	32.5	139.9	24.7	30.9	0.071	0.71	**190.8**	**5.5**
RIC_15_005 (Montoume)														
z1	9.85	43.19	13.250	162.59	4.8	40.1	50.2	176.0	29.7	47.3	0.057	0.77	**211.9**	**6.2**
z2	23.13	106.12	24.94	157.88	4.6	37.4	37.5	244.3	40.8	32.1	0.061	0.75	**209.9**	**6.1**
z3[g]	*2.639*	*21.13*	*11.627*	*85.27*	*2.4*	*26.7*	*30.7*	*120.2*	*25.1*	*23.1*	*0.087*	*0.66*	***130.2***	***3.7***
z4	1.516	8.435	4.151	123.72	3.6	37.0	29.8	169.1	29.0	31.5	0.072	0.71	**174.5**	**5.1**
z5	42.38	177.2	49.24	171.40	4.9	44.7	34.7	258.1	43.7	45.3	0.059	0.76	**225.4**	**6.5**
z6	4.550	23.28	9.180	137.13	3.9	27.7	31.7	154.5	38.4	41.1	0.083	0.67	**204.7**	**5.9**
z7	10.99	56.36	18.06	138.88	4.0	28.9	37.4	139.6	29.7	32.5	0.077	0.69	**200.2**	**5.7**
z8	1.782	11.58	2.036	113.36	3.3	31.7	26.2	118.0	30.8	32.9	0.090	0.65	**175.0**	**5.1**
z9	4.902	22.20	7.258	156.86	4.5	39.2	31.1	119.6	29.0	29.0	0.076	0.70	**225.6**	**6.5**
z10	9.94	50.40	20.48	138.06	3.9	28.3	27.6	127.7	21.6	25.8	0.087	0.66	**210.7**	**5.9**
RIC_15_013 (Babaudus)														
z1	16.12	100.04	32.95	114.8	3.3	32.5	35.1	160.6	32.4	21.5	0.071	0.71	**161.1**	**4.7**
z2[g]	20.66	69.73	19.44	*211.6*	*6.3*	*37.6*	*36.3*	*211.2*	*28.6*	*27.3*	*0.063*	*0.75*	***283.9***	***8.5***
z3	4.176	21.47	16.926	126.2	3.6	28.0	31.0	146.9	31.0	23.0	0.082	0.67	**187.6**	**5.4**
z4[g]	1.222	7.156	10.987	*97.1*	*2.7*	*35.8*	*29.5*	*120.8*	*20.3*	*24.1*	*0.078*	*0.68*	***142.7***	***4.0***
z5	1.879	11.86	5.557	109.7	3.2	23.6	22.9	94.4	12.2	15.1	0.11	0.59	**186.5**	**5.5**
z6[g]	3.026	21.79	11.850	*94.8*	*2.7*	*25.8*	*29.6*	*131.9*	*20.9*	*18.9*	*0.087*	*0.66*	***144.7***	***4.1***
z7	3.013	25.67	7.45	84.6	3.0	23.8	22.9	95.8	14.8	17.7	0.11	0.59	**143.2**	**5.1**
z8	2.354	16.11	7.389	101.5	2.9	23.2	26.2	92.8	16.0	23.1	0.10	0.60	**170.1**	**4.9**
z9	2.555	17.41	8.610	101.2	3.1	34.1	28.3	109.7	18.5	17.5	0.083	0.67	**150.8**	**4.6**

Sample	^{4}He[a]	^{238}U[a]	^{232}Th[a]	$Date_{RAW}$[b]	$2\sigma_{RAW}$[b]	R1[c]	R2[c]	L[c]	H1[c]	H2[c]	B[d]	F_T[e]	$Date_{corr}$[f]	$2\sigma_{corr}$[f]
	10^{11} atoms	10^{11} atoms	10^{11} atoms	Ma	Ma	µm	µm	µm	µm	µm	μm^{-1}	Mean	Ma	Ma
RIC_15_014 (Montoume)														
z1	2.379	10.79	5.244	151.5	4.6	27.7	26.6	129.4	18.0	21.8	0.088	0.65	**232.9**	**7.1**
z2[g]	8.92	74.07	33.74	*83.8*	*2.4*	*50.3*	*39.9*	*174.3*	*38.0*	*36.2*	*0.057*	*0.77*	***109.3***	***3.2***
z3[g]	2.571	19.42	5.928	*95.0*	*3.0*	*34.9*	*40.7*	*121.0*	*30.5*	*24.8*	*0.071*	*0.71*	***133.1***	***4.2***
z4	4.037	22.43	11.480	123.4	3.7	31.8	31.1	108.5	23.4	21.6	0.083	0.67	**184.2**	**5.5**
z5	3.204	12.81	5.585	173.4	5.0	24.6	27.1	140.6	23.1	22.5	0.091	0.64	**270.5**	**7.9**
z6	13.73	59.26	24.88	161.3	4.7	36.5	35.0	172.7	32.6	30.3	0.067	0.73	**221.7**	**6.5**
z7	5.126	27.95	18.20	122.3	3.5	28.1	30.9	137.1	24.2	24.8	0.082	0.67	**182.3**	**5.1**
z8	3.357	14.72	8.609	153.7	4.5	34.5	32.0	164.0	34.5	34.9	0.073	0.71	**217.9**	**6.4**
z9	3.413	18.25	6.154	132.8	3.9	30.3	28.7	147.6	31.5	33.2	0.082	0.67	**197.3**	**5.8**
z10	0.744	4.274	2.199	119.2	4.7	29.7	25.7	107.9	18.9	23.8	0.091	0.64	**186.6**	**7.4**
RIC_15_015 (Montoume)														
z1	4.051	19.14	6.408	150.2	5.1	29.8	28.0	105.5	14.1	21.7	0.088	0.65	**230.3**	**7.8**
z2	1.015	4.421	2.979	152.0	5.1	28.2	24.3	100.1	19.7	18.7	0.097	0.62	**245.7**	**8.3**
z3	2.032	10.46	4.599	135.1	4.6	24.1	27.0	109.7	16.9	26.5	0.097	0.62	**218.1**	**7.4**
z4	1.897	13.59	6.074	97.2	3.2	30.8	24.5	96.7	15.2	17.5	0.094	0.63	**154.0**	**5.1**
z5	1.243	5.338	3.559	154.3	5.3	28.3	28.3	96.7	38.2	24.3	0.098	0.61	**251.4**	**8.6**
z6	1.019	7.71	3.278	92.5	3.1	32.5	23.9	96.4	32.3	20.0	0.097	0.62	**149.5**	**5.0**

[a] These are the absolute concentrations for parent and daughter isotopes used in the age equation. The widely accepted $^{238}U/^{235}U$ ratio of 137.88 was used to calculate ^{235}U.
[b] This is the raw age, calculated iteratively from the age equation, that does not account for alpha ejection, along with the propagated error.
[c] Zircon dimensions. R1 and R2 are perpendicular half-widths, L is the total length, and H1 and H2 are pyramidal termination heights.
[d] Surface area to volume ratio.
[e] Alpha ejection correction factor.
[f] The alpha-ejection corrected age, obtained by dividing the raw age by F_T, along with the propagated uncertainty.
[g] Individual analyses that were excluded from the final inverse-variance weighted mean for ZrnHe in the text via a modified Hampel Identification.

Table S2: ZrnPb laser ablation ICP-MS data from this study.

	$^{207}Pb/^{235}U$[a]	2σ[a]	$^{206}Pb/^{238}U$[a]	2σ[a]	Date $^{206}Pb/^{238}U$[b]	2σ[b]
RIC_15_002 (Montoume)						
z11	0.466	0.065	0.0534	0.0016	335.5	9.5
z12	0.47	0.10	0.0613	0.0033	383	20
z13	0.473	0.045	0.0556	0.0016	348.5	9.6
z14	0.610	0.054	0.0690	0.0027	430	16
z15	0.607	0.038	0.0732	0.0020	455	12
z16	0.663	0.039	0.0806	0.0017	500	10
z17	0.412	0.017	0.0521	0.0010	327.6	5.9
z18	0.662	0.079	0.0724	0.0021	450	13
z19	1.44	0.10	0.1378	0.0031	832	17
z20	0.692	0.053	0.0826	0.0022	512	13
z21	5.19	0.25	0.316	0.012	1765	60
z22	0.619	0.034	0.0715	0.0013	445.2	7.7
z23	1.03	0.16	0.0684	0.0018	426	11
z24	0.557	0.031	0.0634	0.0014	396.3	8.5
z25	0.630	0.028	0.0770	0.0012	478.1	7.0
z26	0.740	0.061	0.0804	0.0038	497	22
z27	0.576	0.034	0.0531	0.0016	333.3	9.6
z28	0.773	0.040	0.0885	0.0012	546.7	7.1
z29	0.735	0.048	0.0633	0.0011	395.6	6.5
z30	1.703	0.070	0.1453	0.0026	874	14
z31	0.405	0.041	0.05223	0.00071	328.2	4.3
z32	0.567	0.044	0.0691	0.0030	430	18
z33	0.745	0.042	0.0897	0.0021	554	12
z34	0.489	0.046	0.0583	0.0017	365	10
z35	0.549	0.067	0.0708	0.0048	440	28
z36	0.731	0.042	0.06869	0.00073	428.2	4.4
z37	0.566	0.021	0.06876	0.00063	428.6	3.8
z38	0.522	0.033	0.05628	0.00092	704.0	9.3
z39	2.46	0.15	0.2022	0.0097	352.9	5.6
z40	0.690	0.035	0.0798	0.0013	1181	52
z41	0.560	0.016	0.06713	0.00065	494.9	7.9
z42	0.617	0.019	0.07611	0.00075	418.8	3.9
z43	0.593	0.019	0.07287	0.00087	453.4	5.2
z44[c]	*0.396*	*0.014*	*0.0320*	*0.0012*	*203.1*	*7.3*
z45	0.514	0.015	0.06406	0.00087	472.8	4.5
z46	0.480	0.056	0.0528	0.0012	400.2	5.2
z47	0.676	0.020	0.0806	0.0010	499.5	5.7
z48	0.603	0.016	0.0748	0.0010	331.7	7.2

	$^{207}Pb/^{235}U$[a]	2σ[a]	$^{206}Pb/^{238}U$[a]	2σ[a]	Date $^{206}Pb/^{238}U$[b]	2σ[b]
z49	0.515	0.023	0.05983	0.00093	465.1	5.8
z50	0.499	0.017	0.0618	0.0010	374.5	5.7
z51	0.527	0.033	0.05648	0.00059	386.7	5.9
z52	0.600	0.030	0.07609	0.00091	354.2	3.6
z53	0.461	0.014	0.05681	0.00063	472.7	5.4
RIC_15_005 (Montoume)						
z11[c]	*391*	*19*	*5.75*	*0.20*	*135*	*20*
z12	0.756	0.054	0.0895	0.0026	552	15
z13	0.577	0.024	0.0711	0.0013	442.4	7.9
z14	0.440	0.020	0.05624	0.00067	352.7	4.1
z15	0.463	0.030	0.0563	0.0021	353	13
z16	0.703	0.043	0.08340	0.00091	516.4	5.4
z17	0.714	0.041	0.0909	0.0015	561.0	9.1
z18	0.694	0.031	0.07381	0.00089	459.0	5.4
z19	0.493	0.046	0.0497	0.0013	312.3	8.3
z20	0.615	0.030	0.0726	0.0017	451	10
z21	0.754	0.053	0.0739	0.0015	459.6	9.0
z22	0.76	0.12	0.097	0.021	590	120
z23	0.90	0.15	0.0747	0.0024	464	14
z24	0.764	0.022	0.0924	0.0009	569.6	5.3
z25	0.778	0.046	0.0897	0.0011	555.6	7.4
z26	0.483	0.023	0.0600	0.0018	376	11
z27	0.663	0.058	0.0664	0.0013	414.3	7.6
z28	0.471	0.013	0.0469	0.0014	295.5	8.7
z29	0.717	0.053	0.0718	0.0020	447	12
z30	2.27	0.74	0.0726	0.0085	449	50
z31	0.652	0.027	0.07475	0.00082	464.7	4.9
z32	0.656	0.055	0.0371	0.0010	235.0	6.3
z33	0.632	0.038	0.0727	0.0013	452.6	8.1
z34	0.658	0.030	0.07945	0.00089	492.8	5.3
z35	0.365	0.019	0.0419	0.0013	264.4	7.9
z36	0.501	0.031	0.0613	0.0020	384	12
z37[c]	*0.814*	*0.070*	*0.0298*	*0.0011*	*189.2*	*6.6*
z38	0.522	0.017	0.05584	0.00072	270.1	3.4
z39	0.575	0.016	0.0508	0.0010	319.4	6.4
z40	0.443	0.016	0.04231	0.00059	350.2	4.4
z41	0.3715	0.0078	0.04247	0.00053	267.1	3.7
z42	0.3550	0.0075	0.04427	0.00051	268.1	3.3
z43	0.492	0.019	0.05627	0.00067	279.2	3.1
z44	0.434	0.015	0.05260	0.00087	352.9	4.1

					Date	
	$^{207}Pb/^{235}U$[a]	2σ[a]	$^{206}Pb/^{238}U$[a]	2σ[a]	$^{206}Pb/^{238}U$[b]	2σ[b]
z45	0.384	0.013	0.04275	0.00048	330.4	5.3
z46	0.3699	0.0079	0.03998	0.00022	252.7	1.3
z47	0.521	0.016	0.05978	0.00056	374.3	3.4
z48	0.594	0.014	0.0723	0.0015	269.8	3.0
z49	0.742	0.014	0.09009	0.00069	449.9	8.9
z50	0.634	0.015	0.07097	0.00051	556.0	4.1
z51	0.609	0.023	0.07352	0.00046	457.3	2.8
z52	0.510	0.015	0.04594	0.00052	442.0	3.1
z53	0.647	0.065	0.0516	0.0013	282.6	3.0
z54	0.3555	0.0075	0.04481	0.00048	342.0	3.2
z55	0.372	0.010	0.03644	0.00091	324.4	8.2
z56	0.368	0.012	0.04464	0.00040	230.7	5.6
z57	1.214	0.026	0.1154	0.0016	281.5	2.5
RIC_15_013 (Babaudus)						
z10	0.808	0.041	0.08921	0.00076	550.8	4.5
z11	0.898	0.058	0.0904	0.0011	557.9	6.5
z12	1.153	0.044	0.09199	0.00082	567.2	4.9
z13	3.83	0.52	0.0934	0.0055	575	32
z14	1.418	0.051	0.0575	0.0034	360	21
z15	1.910	0.078	0.0826	0.0023	512	14
z16	5.00	0.44	0.0967	0.0034	594	20
z17	1.254	0.066	0.0571	0.0011	357.9	6.4
z18	3.5	1.3	0.083	0.017	505	93
z19	1.75	0.14	0.0471	0.0015	296.6	9.4
z20	7.17	0.56	0.1123	0.0041	685	23
z21	2.44	0.12	0.1120	0.0019	684	11
z22	2.07	0.35	0.0676	0.0026	421	15
z23	2.06	0.23	0.0660	0.0039	411	24
z24	5.8	1.1	0.1137	0.0097	689	54
z25	1.044	0.036	0.04279	0.00055	392.7	5.7
z26	2.180	0.083	0.05430	0.00049	340.9	3.0
z27	3.14	0.11	0.06282	0.00094	372.6	5.8
z28	2.39	0.12	0.0595	0.0010	580.0	6.8
z29	2.49	0.11	0.0942	0.0011	268.6	3.3
z30	1.88	0.14	0.06087	0.00068	380.9	4.1
z31	1.233	0.069	0.04254	0.00053	494.1	9.7
z32	3.13	0.16	0.0797	0.0016	445	15
z33	2.14	0.10	0.0715	0.0025	231.6	2.1
z34	3.72	0.10	0.05559	0.00051	321.6	3.5
z35	2.760	0.074	0.05116	0.00058	257.0	3.6

	$^{207}Pb/^{235}U$[a]	2σ[a]	$^{206}Pb/^{238}U$[a]	2σ[a]	Date $^{206}Pb/^{238}U$[b]	2σ[b]
z36	3.062	0.066	0.2522	0.0015	389.7	5.2
z37	1.272	0.043	0.04067	0.00058	1449.8	7.8
z38	3.079	0.048	0.05379	0.00043	337.7	2.6
z39	4.37	0.16	0.0743	0.0012	461.8	6.9
z40	2.210	0.034	0.04553	0.00034	287.0	2.1
z41	1.943	0.048	0.04549	0.00047	286.8	2.9
z42	1.754	0.079	0.06090	0.00088	381.1	5.3
z43	2.148	0.086	0.09859	0.00087	606.1	5.1
z44	0.884	0.030	0.03659	0.00034	348.7	3.1
z45	1.972	0.052	0.05553	0.00071	348.3	4.3
z46	1.710	0.080	0.08087	0.00055	501.3	3.3
RIC_15_014 (Montoume)						
z11	0.631	0.029	0.07901	0.00094	490.1	5.6
z12[c]	*0.441*	*0.013*	*0.03031*	*0.00057*	*192.5*	*3.5*
z13	0.466	0.039	0.0482	0.0017	303	10
z14	24.3	3.3	0.262	0.028	1460	140
z15	0.540	0.032	0.0660	0.0014	412.1	8.7
z16	0.467	0.020	0.0534	0.0013	335.1	8.0
z17[c]	*0.406*	*0.012*	*0.03301*	*0.00077*	*209.3*	*4.8*
z18	0.641	0.045	0.0772	0.0012	479.2	7.4
z19	0.375	0.012	0.04100	0.00039	259.0	2.4
z20[c]	*0.3809*	*0.0093*	*0.0334*	*0.0014*	*211.7*	*8.5*
z21	0.933	0.084	0.1041	0.0030	638	17
z22	3.86	0.31	0.241	0.014	1382	72
z23	0.529	0.023	0.0652	0.0011	407.0	6.5
z24	0.649	0.033	0.07991	0.00072	495.5	4.3
z25	4.15	0.17	0.2465	0.0080	1417	42
z26	0.509	0.028	0.0628	0.0010	392.3	6.1
z27	0.498	0.016	0.0617	0.0010	385.8	5.8
z28	0.444	0.019	0.05461	0.00077	342.7	4.7
z29	0.584	0.032	0.06232	0.00086	293.2	7.2
z30	0.447	0.014	0.04991	0.00070	313.9	4.3
z31	0.427	0.028	0.04885	0.00065	307.5	4.0
z32	0.418	0.017	0.04552	0.00080	286.9	5.0
z33	0.619	0.018	0.0755	0.0011	469.4	6.6
z34	0.342	0.011	0.04834	0.00048	304.3	3.0
z35	0.618	0.042	0.05920	0.00062	370.8	3.8
z36	0.554	0.027	0.06901	0.00064	430.2	3.9
z37	0.666	0.030	0.0775	0.0014	481.0	8.4
z38	0.543	0.015	0.06469	0.00089	404.0	5.4

	$^{207}Pb/^{235}U$[a]	2σ[a]	$^{206}Pb/^{238}U$[a]	2σ[a]	Date $^{206}Pb/^{238}U$[b]	2σ[b]
z39	0.560	0.037	0.03969	0.00090	250.9	5.6
z40	0.538	0.020	0.05696	0.00056	357.1	3.4
z41	0.387	0.015	0.03898	0.00061	246.5	3.8
z42	0.485	0.010	0.04308	0.00036	271.9	2.2
z43	11.12	0.17	0.4473	0.0041	2386	17
z44	0.961	0.027	0.07050	0.00062	439.1	3.7
z45	0.429	0.018	0.05457	0.00071	342.5	4.3
z46	0.418	0.017	0.03820	0.00041	241.7	2.5
z47	0.310	0.010	0.03833	0.00033	242.5	2.0
RIC_15_015 (Montoume)						
z7	0.358	0.021	0.03815	0.00039	241.3	2.4
z8	0.420	0.014	0.04388	0.00095	276.8	5.8
z9	0.796	0.047	0.08269	0.00088	512.1	5.2
z10	9.95	0.19	0.4478	0.0033	2385	15
z11	0.396	0.044	0.04382	0.00087	276.4	5.4
z12	0.673	0.023	0.0760	0.0013	471.9	8.0
z13	0.647	0.042	0.07264	0.00071	452.0	4.3
z14	0.93	0.34	0.0559	0.0054	350	32
z15	1.79	0.16	0.152	0.010	904	57
z16	0.727	0.072	0.0781	0.0017	485	10
z17	0.637	0.047	0.0755	0.0051	468	30
z18	0.47	0.11	0.0506	0.0022	318	13
z19	0.497	0.057	0.0484	0.0024	304	15
z20	0.645	0.054	0.0719	0.0013	447.3	7.6
z21	0.573	0.035	0.0683	0.0020	426	12
z22	0.662	0.015	0.07217	0.00044	449.2	2.7
z23	0.413	0.021	0.0420	0.0010	264.9	6.0
z24	0.523	0.022	0.06448	0.00091	402.8	5.5
z25[c]	*0.398*	*0.011*	*0.03302*	*0.00044*	*209.4*	*2.8*
z26	0.566	0.015	0.06830	0.00077	425.9	4.6
z27	0.546	0.011	0.06284	0.00085	392.8	5.2
z28	0.606	0.015	0.07282	0.00072	453.1	4.3
z29[c]	*0.377*	*0.058*	*0.03150*	*0.00069*	*199.9*	*4.3*
z30	0.696	0.014	0.08190	0.00086	507.4	5.1
z31	0.482	0.014	0.04511	0.00091	284.4	5.6
z32[c]	*0.308*	*0.018*	*0.03190*	*0.00041*	*202.4*	*2.6*
z33	0.3134	0.0089	0.03679	0.00047	232.9	2.9

[a] Corrected U/Pb ratios and uncertainties from the ICP-MS.
[b] Final $^{206}Pb/^{238}U$ age and uncertainty, processed in IGOR Pro using the Plešovice zircon as an age standard.

[c] The nine youngest zircons from the whole dataset. The RIC_15_005_z11 date of 135 Ma is a clear outlier in the data and was not used in the mean for our proposed ZrnPb impact age.

Table S3. ZrnRD data for all samples.

Sample	**FWHM**[a]	**1σ**[a]	**C_U**[b]	**2σ**[b]	**C_{Th}**[b]	**2σ**[b]	**Da**[c]	**2σ**[c]	**Date**[d]	**2σ**[d]
	cm^{-1}	cm^{-1}	ppm	ppm	ppm	ppm	10^{-17} α/mg	10^{-17} α/mg	Ma	Ma
RIC_15_002 (Montoume)										
z54	9.78	0.49	605	36	409.2	1.4	5.84	0.75	251	34
z55	7.55	0.38	104.7	6.3	58.0	8.9	4.34	0.53	1030	120
z56	9.80	0.49	212	13	36.9	5.6	5.86	0.75	760	99
z57	8.59	0.43	575	35	328	50	5.02	0.63	233	32
z58	8.45	0.42	263	16	135	21	4.93	0.62	493	65
z59	9.00	0.45	282	17	89.7	0.6	5.30	0.67	513	68
z60	12.26	0.61	1930	120	1002.5	1.0	7.7	1.0	108	16
z61	10.39	0.52	453	27	290.9	1.3	6.28	0.82	359	49
z62	8.91	0.45	300	18	132	20	5.24	0.66	466	62
z63	9.38	0.47	292	18	87	13	5.56	0.71	523	70
z64	7.36	0.37	90.8	5.5	93	14	4.21	0.52	1050	130
RIC_15_005 (Montoume)										
z58	6.66	0.33	144.3	8.6	89	14	3.77	0.46	662	83
z59	9.42	0.47	324	20	191	29	5.59	0.71	449	60
z60	8.90	0.45	322	19	221	34	5.23	0.66	416	55
z61	9.78	0.49	302	18	203	31	5.84	0.75	493	67
z62	13.38	0.67	1425	86	722	111	8.6	1.2	164	24
z63[e]	*15.83*	*0.79*	*1444*	*87*	*511*	*78*	*10.7*	*1.6*	*207*	*32*
z64	8.31	0.42	333	20	143	22	4.84	0.60	392	52
z65	9.40	0.47	348	21	182	28	5.58	0.71	424	57
z66[e]	*12.20*	*0.61*	*785*	*47*	*1205*	*184*	*7.6*	*1.0*	*216*	*31*
z67	8.09	0.40	170	10	67	10	4.69	0.58	725	92
z68	8.24	0.41	604	36	272	42	4.79	0.60	217	29

Sample	FWHM[a]	1σ[a]	C_U[b]	2σ[b]	C_{Th}[b]	2σ[b]	Da[c]	2σ[c]	Date[d]	2σ[d]
	cm^{-1}	cm^{-1}	ppm	ppm	ppm	ppm	10^{-17} α/mg	10^{-17} α/mg	Ma	Ma
z69[e]	*11.10*	*0.56*	*829*	*49*	*402*	*61*	*6.80*	*0.90*	*223*	*32*
z70[e]	*8.85*	*0.44*	*660*	*39*	*513*	*78*	*5.20*	*0.66*	*202*	*27*
z71	6.40	0.32	156.6	9.3	85	13	3.60	0.43	597	75
z72[e]	*16.41*	*0.82*	*1566*	*94*	*498*	*76*	*11.2*	*1.7*	*203*	*32*
z73	6.68	0.33	168	10	96	15	3.78	0.46	580	74
z74	13.85	0.69	1628	97	660	100	9.0	1.3	153	22
z75	10.90	0.55	659	40	266	41	6.65	0.87	277	38
z76	9.08	0.45	486	29	177	27	5.36	0.68	304	41
RIC_15_013 (Babaudus)										
z47	9.09	0.45	344	21	186	28	5.36	0.68	410	55
z48	6.15	0.31	154.4	9.2	100	15	3.45	0.41	568	73
z49	7.89	0.39	750	45	295	45	4.56	0.56	169	22
z50	8.35	0.42	337	20	230	35	4.86	0.61	371	49
z51	6.93	0.35	144.4	8.6	54.9	8.4	3.94	0.48	721	90
z52	6.29	0.31	332	20	160	25	3.54	0.43	287	37
z53	6.31	0.32	186	11	92	14	3.55	0.43	502	63
z54	5.97	0.30	246	15	76	12	3.34	0.40	376	48
z55	7.22	0.36	339	20	178	27	4.12	0.50	324	43
z56	8.56	0.43	1030	61	328	50	5.00	0.63	137	19
z57	8.56	0.43	789	47	296	45	5.00	0.63	177	24
z58	6.21	0.31	126.9	7.6	75	11	3.49	0.42	699	89
z59	6.34	0.32	182	11	153	23	3.57	0.43	483	61
z60[e]	*18.25*	*0.91*	*1618*	*98*	*860*	*130*	*13.07*	*2.08*	*217*	*36*
z61	8.11	0.41	276	16	160	25	4.70	0.58	445	58

Sample	FWHM[a]	1σ[a]	C_U[b]	2σ[b]	C_{Th}[b]	2σ[b]	Da[c]	2σ[c]	Date[d]	2σ[d]
	cm^{-1}	cm^{-1}	ppm	ppm	ppm	ppm	10^{-17} α/mg	10^{-17} α/mg	Ma	Ma
RIC_15_014 (Montoume)										
z48	9.06	0.45	227	14	149	23	5.34	0.68	595	79
z49	7.80	0.39	250	15	166	25	4.50	0.56	461	61
z50	9.76	0.49	332	19	166	26	5.83	0.75	465	61
z51	7.06	0.35	160	10	78	12	4.02	0.49	654	84
z52	11.36	0.57	590	35	254	39	6.99	0.93	322	45
z53	6.49	0.32	139.2	8.4	97	15	3.66	0.44	656	81
z54	6.17	0.31	68.8	4.1	49.8	7.6	3.46	0.42	1190	140
z55	7.20	0.36	217	13	153	23	4.11	0.50	481	63
z56	12.41	0.62	1264	76	315	48	7.8	1.1	177	25
z57	12.11	0.61	894	53	201	31	7.6	1.0	243	34
z58	8.29	0.41	111.6	6.7	82	13	4.82	0.60	1000	130
z59	7.42	0.37	432	26	166	25	4.25	0.52	272	36
z60	7.14	0.36	298	18	185	28	4.07	0.50	356	46
RIC_15_015 (Montoume)										
z34	18.72	0.94	598	36	301	46	13.6	2.2	592	98
z35[e]	*8.02*	*0.40*	*550*	*33*	*592*	*90*	*4.64*	*0.58*	*204*	*27*

[a] Corrected FWHM using the Irmer (1985) equation. For error propagation, all FWHM values were given a notional 1σ of 5% (Pidgeon et al. 2014).
[b] Absolute concentrations of the isotopes with uncertainties; calculated using a customized, homogenous synzircon of known U-Th concentrations.
[c] Alpha dose with propagated uncertainties. Calculated from the Palenik (2003) equation reported in text using the corrected FWHM value.
[d] Radiation damage ages iteratively calculated in MATLAB using the Nasdala et al. (2001) equation reported in text (Equation 1), along with uncertainties derived from a Monte Carlo simulation.
[e] Subpopulation of impact-aged zircons used for the ZrnRD inverse-variance weighted mean reported in text.